VISCOELASTIC AND FATIGUE PROPERTIES OF DENTAL ADHESIVES AND THEIR IMPACT ON DENTIN-ADHESIVE INTERFACE DURABILITY

By

Viraj Singh

Submitted to the graduate degree program in Mechanical Engineering and the Graduate Faculty of University of Kansas in partial fulfillment of the requirements for the degree of
Master of Science

Chairperson _____ Dr Anil Misra

Committee Members* _____*
Dr Paulette Spencer

_____*
Dr Sarah L. Kieweg

Date Defended: _____

The Thesis Committee for Viraj Singh certifies
that this is the approved Version of the following thesis:

VISCOELASTIC AND FATIGUE PROPERTIES OF DENTAL ADHESIVES AND THEIR IMPACT ON DENTIN-ADHESIVE INTERFACE DURABILITY

Committee:

Chairperson: Dr Anil Misra

Dr Paulette Spencer

Dr Sarah L Kieweg

Date Approved: _____

ABSTRACT

The clinical performance of composite tooth restoration under cyclic loading is impacted by the behavior of the dentin-adhesive (d-a) interface, which is a complex construct of different material components. Dentin adhesive is a significant material component of the d-a interface. Creep, fatigue and monotonic tests were performed to characterize the mechanical properties of a dentin adhesive in dry and wet conditions. These properties were utilized along with a 3d micromechanical finite element (FE) model to develop a methodology for predicting the durability behavior of the d-a interface.

Experimental results showed that the dentin adhesives have rate-dependent behavior and their properties deteriorate in the presence of water. FE calculations showed that, different material components experience different stress concentrations depending upon the microstructure. The durability of the d-a interface was found to be a function of both the microstructure and adhesive properties.

TABLE OF CONTENTS

LIST OF TABLES

LIST OF FIGURES

ACKNOWLEDGEMENT

First, I would like to thank, Dr Anil Misra and Dr Paulette Spencer for their constant support, invaluable guidance and giving me the opportunity to work on this project. If not for the suggestions and help given by them, this project could have never been possible

I also wish to express my gratitude towards Dr Sarah L. Kieweg for serving on my graduate committee and providing me useful suggestions.

I would especially like to thank Dr Qiang Ye and Dr Jonggu Park for giving me valuable advice and spending countless hours helping me in the laboratory work involved in this project.

I also thank my fellow classmates and my lab mates Orestes Marangos, Ranganathan Parthsarathy, and Shiping Huang for their time to time help through out this project.

Lastly, and most importantly I express my forever gratitude to my parents and family members. I thank them for their love, emotional support and for all they have done for me. This thesis is dedicated to them.

1.0 INTRODUCTION AND LITERATURE REVIEW

1.1 MOTIVATION AND OBJECTIVES

In the United States 166 million dental restorations are completed each year and nearly two-thirds of these restorations fail prematurely [1-2]. There are several factors that contribute to this premature failure, including chemical degradation, biological factors and mechanical failure. Hence it is important to systematically study these factors to better understand dental restoration failure.

Mechanical failures can be broadly classified into two categories: static and fatigue failure. Static failures are due to monotonically applied loads, while fatigue failures occur under repeated or cyclic loading. Masticatory loads/forces consist of both static and cyclic. Cyclic loads occur with an average frequency of 0.1Hz. There is evidence [3] that the cyclic nature of loads/stresses in the mouth is a key factor contributing to the premature failure of dental composite restorations. Thus it is important to determine the behavior of the composite restoration under cyclic loading. While the degradation and fatigue properties of dental composites have been studied more widely[4], limited studies have been performed to investigate the fatigue life at the dentin-composite interface [5-6].

The dentin adhesive joins the composite material to the subjacent tooth structure forming a complex construct of different material components. In composite tooth restoration the dentin-adhesive (d-a) interface is a particularly critical area. Chemical, structural and mechanical degradation at this interface are major factors contributing to

premature failure of the composite restoration. Since cyclic loading is representative of the stresses that occur on the composite restoration in vivo, it is necessary to study the failure of d-a interface under cyclic loading. Clearly, the life of the d-a interface depends in part on the mechanical properties of the dentin adhesive.

To understand the mechanical behavior of the adhesive under cyclic loading requires characterization of the viscoelastic and fatigue properties of the material. The objective of the current study is to (1) characterize the viscoelastic and fatigue properties of dentin adhesives in dry and wet conditions, and (2) to use these data to predict the fatigue life of the d-a interface.

To achieve our first objective, we perform creep, fatigue and monotonic tests on dentin adhesive samples in dry and wet conditions using a dynamic mechanical analyzer. To achieve our second objective we developed a 3d linear elastic micromechanical finite element model of the dentin- adhesive interface. The FE calculations show that under an applied loading, the stresses experienced by the individual material components of d-a interface are different depending upon the microstructure. Therefore, the individual components will have particular fatigue life based upon their corresponding stress-cycle (S-N) curves. Overall fatigue failure of the dentin-adhesive interface will depend on the material component having the lowest fatigue life at particular applied stress amplitude. Hence, all the individual curves of the different material components are combined to give the overall S-N curve of the dentin-adhesive interface.

In this approach it is critical to have correct S-N curves for the individual material components. S-N curves for dentin and collagen were taken from the literature [7-9], while that for the dentin adhesive was obtained from objective 1 since there is limited fatigue data available in the literature for dentin adhesives.

1.2 LITERATURE REVIEW

It is very difficult to complete mechanical property measurements on the tooth in vivo due to the nature of loading, environmental conditions and geometry. Hence to better understand the mechanical behavior of teeth under different loading conditions various authors have performed finite element analyses (FEA). Rodrigues et al. [10] have used micro XCT images to develop a 3d model of the tooth. This model was then used to do a finite element analysis (FEA) of a class 1 restoration. The FEA used linear elastic properties and output was analyzed in the form of maximum principle and maximum shear stress. The key points of this work were as follows: deviation between the micro XCT images and 3d model was less than 0.6% and stress concentration was found in the vicinity of the dentin-composite interface. No information about the convergence of the mesh is mentioned in the presentation of this work. This investigation assumed a perfect bond between dentin and composite and did not include a transition layer (interfacial layer) which connects dentin to composite.

Wakabayashi et al. [11] have reviewed the development and application of nonlinear finite element method in dentistry. This review focused on the following areas; plastic and viscoelastic behavior, tooth-to-tooth contact, and interfacial stress in restorations. Again in most of the reviewed works, interfacial layer was typically not incorporated in the FE models rather the researchers assumed perfect bonding between different materials, e.g. composite, adhesive and tooth structure. The main findings from this work [11] were that compressive stresses developed perpendicular to the tooth-restoration interface in the cavity while tensile stress was oblique to the interfacial planes. Hence we should not compare the maximum tensile stress with the tensile bond strength because tensile bond strength is measured under a tensile load that is perpendicular to the bonded surface.

In a separate study Yettram et al. [12] developed a 2d model of a buccolingual slice of a mandibular second premolar with amalgam restoration. In this work, the investigators developed models with isotropic and orthotropic enamel properties. Further they studied a tooth restored with a full gold-alloy crown and predicted that failure could occur at the gold-cement interface.

In another study by Ausiello et al. [13] a 3d linear elastic finite element model was used to demonstrate premature failure due to occlusal loading and polymerization shrinkage. The FE model had 7282 brick (8 node) and tetrahedral (4 node) elements. The investigators included an interfacial layer between the composite and dentin. The adhesive interface was modeled using spring elements having normal and shear stiffness given by the relationship $K_i=A_iE/L$ and $K_i=A_iG/L$ where E is the Young's modulus of adhesive, G is the shear modulus of adhesive and L is the thickness of interface. FE model showed that axial test tooth fracture occurs between 700 and 800N and under occlusal loading the crack starts at the top of the adhesive layer. The authors concluded that a thicker adhesive layer would limit the intensity of the stress that is transmitted to the natural tooth. The authors reported that the thick layer of adhesive will absorb the stresses associated with deformation of the composite. Furthermore, the authors reported that a thick layer of lower elastic modulus adhesive exhibits the same rigidity as a thick layer of higher elastic modulus adhesive. The interface modeled using the spring is not accurate because stiffness of spring elements depends upon E and L. If we decrease or increase both E and L then there is no change in the stiffness of the interface hence no change in stress distribution in the composite restoration.

Previously Frankenberger et al. [14-15] evaluated the effectiveness of various dentin adhesives using quasistatic and dynamic dentin bond tests. The authors performed cyclic fatigue tests at 5mm/min up to 5000 cycles or until the specimen failed. If the sample survived 5000 cycles, stress for the subsequent specimens was increased. The limitation with

this study was that information about the mechanical properties of pure dentin adhesives was not acquired. Rather the results were based on the bonded system that includes demineralized and mineralized dentin as well as the adhesive. Secondly strength based upon the static push out test is not a true measure of the strength of the material. Also, the authors performed the static bond tests at only 5mm/min loading, but dentin adhesives are viscoelastic materials and thus, their strength depends upon the rate of loading. Moreover fatigue tests were performed using staircase method [16] only for 5000 cycles which is not enough to characterize the life of pure dentin adhesives.

In a separate investigation, Staninec et al. [5] studied the cyclic fatigue properties of composite-dentin bonds using four point bend tests. The authors prepared $0.8 \times 0.87 \times 10$ mm rectangular beam specimens of dentin bonded to composite. Static tests were performed on dentin, composite and dentin-composite beams to find fracture strengths. After that, fatigue tests were performed for composite-dentin beams at a stress ratio of 0.1. The authors reported that all the specimens failed adhesively. At a maximum bending stress of 89.9MPa the dentin-composite bond lasted for only 16 cycles, whereas at stress of 49.2 it lasted for 10^6 cycles which according to author means no fracture.

2.0 DENTAL ADHESIVES MECHANICAL PROPERTIES

Mechanical tests like monotonic, creep and fatigue are required to characterize the mechanical behavior and durability of any type of engineering material. Similarly to characterize the viscoelastic and fatigue properties of dentin adhesives we have performed stress-strain, creep and fatigue experiments. The environment inside the mouth is aqueous hence the above mentioned tests were also performed in wet conditions.

2.1 INSTRUMENTATION

For all the mechanical tests, the TA Q800 Dynamic Mechanical Analyzer (TA Instruments, New Castle, USA) is used. The TA Q800 DMA (Manual, TA instrument) is a thermal analytical instrument used to test the mechanical properties of many different materials. To make the measurement, the test specimen is mounted on one of the several clamps (10mm 3 point bend clamp for all type of mechanical tests in our study as shown in figure 2:1 a and b), then deformation is applied on the specimen to obtain the intrinsic as well as extrinsic mechanical properties. The DMA comprises of:

- **Mechanical section enclosure**: It contains the air bearing, optical encoder, drive motor and associated electronics.

- **Clamp assembly**: Interchangeable clamps for making mechanical measurements in variety of deformation modes to accommodate a wide range of sample shapes and materials.
- **Furnace assembly**: Provides envelop around the clamp assembly and controls the temperature. Temperature is monitored using a thermocouple.
- **Touch Screen**: It allows the operator to monitor and control some of the features like setup, start, stop or reject experiments. The touch screen enhances the overall ease of use and displays valuable information during setup, calibration and experimentation.

The TA Q800 Dynamic Mechanical Analyzer is a precision instrument designed to measure mechanical and viscoelastic properties of rigid and soft solid materials. The sample is mounted on the clamp, one part of which is stationary while the other is movable and connected to the drive motor. Thus, the motor directly affects the deformation of the sample. The drive motor is used to deliver force or stress to the moving drive block. This motor is non-contact in nature i.e. fixed motor assembly is not physically in contact with the movable drive block. The optical encoder measures the resulting displacement of the moving drive block. For smooth, noise-free and continuous delivery of force, the moving drive block is suspended by an air bearing.

The TA Q800 DMA has the following features:

- Operates over a temperature range of -145°C to 600°C, using heating rates up to 20°C/min.
- Determines changes in sample properties resulting from changes in temperature, time, frequency, force, and strain.
- Uses samples that can be in bulk solid, film, fiber, gel, or viscous liquid form.
- Employs interchangeable clamps allowing you to measure many properties, including: modulus, damping, creep, stress relaxation, glass transition, and softening points.

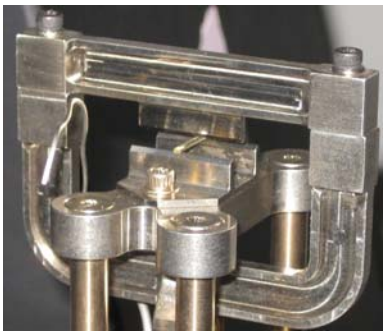

(a)

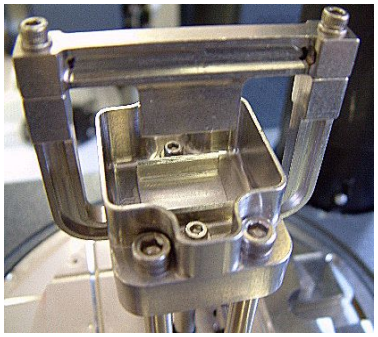

(b)

Figure 2:1 Types of clamp used in mechanical testing
(a) 10mm 3 point bend clamp (b) 10mm 3 point bend submersion clamp

2.2 MATERIALS

The dentin adhesive (polymer) used in this study was made from a resin which was a mixture of two monomers (see Figure 2:2): (1) 2,2-bis[4-(2-hydroxy-3-methacryloxypropoxy) phenyl]-propane (BisGMA, Polysciences Warrington PA), and (2) 2-hydroxyethyl methacrylate (HEMA, Acros Organics, NJ). The two monomers were mixed in mass ratio of 55 % BisGMA and 45% HEMA. A three component photo-initiator system of camphorquinone (CQ), diphenyliodonium hexafluorophosphate (DPIHP) and ethyl-4-(dimethylamino) benzoate (EDMA) was added to expedite the polymerization reaction. Photo-initiator absorbs light and produces free radical which starts the polymerization reaction. All the three components of photo-initiators were added in 0.5% by mass ratio. The mixture of above mentioned components was kept in the shaker for 48hrs and turned upside down every 8hrs so that the mixture was homogenous.

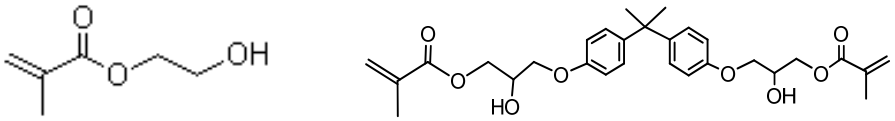

(HEMA) (BisGMA)

Figure 2:2 Monomers used to make resin

2.3 SAMPLE PREPARATION

Circular beam specimens of diameter 1mm and length 15mm (Fgure 2:3.) were made by curing the resin in a glass-tubing mold (Fiber Optic Center Inc, #CV1012, Vitrocom Round Capillary Tubing of Borosilicate Glass). The outer diameter of the glass tubing was 1.2mm (i.e. thickness of the glass tubing mold is 0.1mm). Resin was injected inside the glass tubing using a micro-pipette. After this the adhesive resin was light-cured for 8-9 seconds at room temperature with a LED light curing unit (LED Curebox, Proto-tech, and Portland, OR, USA). The polymerized samples were stored at room temperature for 2 days in a dark room to provide adequate time for post-cure polymerization of the adhesive. The specimens were then stored for 5 days in a vacuum oven in the presence of a drying agent at 37^{o} C to remove water that may have been absorbed during specimen preparation. For mechanical testing in wet conditions adhesive specimens were kept submerged in the distilled water for at least 5 days at 37^{o} C.

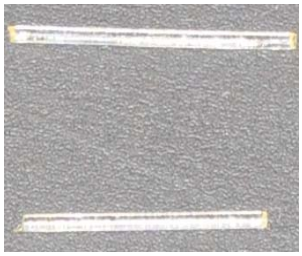

Figure 2:3 Adhesive Circular Beam Specimens

2.4 DEGREE OF CONVERSION

Degree of conversion (DC) quantifies how much monomer is reacted and changed to polymer. To determine the degree of conversion Raman spectroscopy was performed on the specimens using a LabRAM ARAMIS Raman spectrometer (LabRAM HORIBA Jobin Yvon, Edison, New Jersey) with a HeNe laser (λ=633 nm, a laser power of 17 mW) as an excitation source [17-18]. The instrument settings were as follows: 200 μm confocal hole, 150 μm wide entrance slit, 600 gr/mm grating, and 10x objective Olympus lens. Data processing was performed using LabSPEC 5 (HORIBA Jobin Yvon).6. The specimens were mounted on x-y stage using a high precision computer-controlled joystick; the z component of the stage was adjusted with the joystick until the specimen was in focus. To determine the DC, spectra of the uncured resins and beam specimens were acquired over a spectrum range of 700 – 1800 cm^{-1}. The change of the band height ratios of the aliphatic carbon-carbon double bond (C=C) peak at 1640 $cm^{-1}$and the aromatic C=C at 1610 cm^{-1} (phenyl) in both the cured and uncured states was monitored. DC was calculated using the following equation based on the decrease in the intensity band ratios before and after light curing.

$DC\ (\%) = 100[1- (R_{cured}/R_{uncured})]$, R = (band height at 1640 cm^{-1}/band height at 1610 cm^{-1})

The average value of DC was obtained from three readings from different positions on the same sample.

2.5 MECHANICAL TESTS

All the mechanical testes were performed in both dry and wet conditions using a 10 mm three point bending clamp (Figure 2:1) and temperature for all the tests were maintained at 37^{o} C.

2.5.1 Creep

Elastic strains appear instantly upon the application of stress or force but further deformation that occurs gradually with time is called creep strain. Significant amount of creep strain can occur in polymers even below its glass transition temperature T_g[19], therefore it is critical to do creep tests for dentin adhesive polymers. The most common method of creep testing is to apply a constant stress instantaneously and measure the strain over time while keeping the stress constant. We have performed the creep tests at 4 different stress-levels (80 MPa, 55MPa, 48.8 MPa and 30.5MPa) and (30.5 MPa, 24.4 MPa, 18.8 MPa and 12.2 MPa) for dry and wet conditions, respectively

To perform the creep test, the sample was placed on the clamp and a small preload was applied so that the sample does not move from the clamp. Subsequently, a constant stress was applied instantaneously for 120 minutes, after that stress was removed and the sample was allowed to recover for 30 minutes. Strain is measured throughout the whole process. For each stress-level two samples were tested. In total 16 creep tests were performed for both dry and wet conditions.

2.5.2 Static

Static or monotonic tests were performed on dentin adhesives in both dry and wet conditions to find the stress-strain curves. During the static tests, load was applied at a constant rate until the sample broke and the displacement was measured throughout the process**.** In our study we have performed the static tests at three different loading rates of 10N/min, 0.1N/min and 0.0075N/min because dentin adhesives are viscoelastic materials and therefore load-displacement curve depends upon the rate of loading. For upper two loading rates three specimens were tested and two specimens were tested for 0.0075N/min loading

rate. The high loading rate was determined from the machine limits, while the low loading rates was based up the time needed for completion of a test. The intermediate loading rate was chosen arbitrarily.

2.5.3 Fatigue

A material can fail at a stress below its ultimate strength because of damage accumulation during cyclic loading. This phenomenon of failure is called fatigue failure. Fatigue tests can be done using either of two approaches, stress based approach or strain approach. We have used the stress based approach to perform the fatigue testing for both dry and wet dentin adhesives. The applied cyclic stress during a fatigue test is illustrated in Figure 2.4.

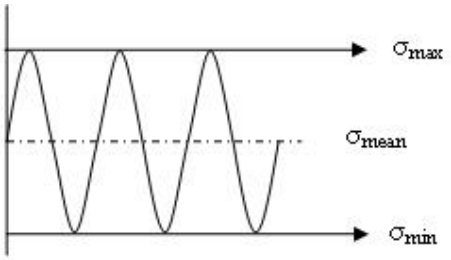

Figure 2:4 Cyclic loading during fatigue test

Stress Ratio: $R= \sigma_{min}/ \sigma_{max}$

Stress Amplitude: $\sigma_a= (\sigma_{max}- \sigma_{min})/2$

Mean Stress: $\sigma_{mean}= (\sigma_{max}+\sigma_{min})/2$

All the fatigue tests were done at a stress ratio R of 0.1 because it gives us broad range of testing and minimizes the effect of mean stress on the sample. In this case, the mean stress and stress amplitude are related as follows: $\sigma_{mean} = \sigma_a \frac{11}{9}$, while the maximum stress is given by $\sigma_{max} = \sigma_a \frac{20}{9}$. The frequency for all fatigue tests was 5Hz.

Stress amplitudes for fatigue testing were decided based upon the stress-strain curves obtained from static tests. Stress amplitudes were such, so that maximum stress over a cycle during the fatigue loading should be smaller then the yield stress (value of stress at which material deviates from its linear stress-strain relationship and becomes nonlinear). This was important because we did not want the specimen to have permanent deformation due to the peak stresses over a cycle. Stress amplitudes and mean stresses for dry tests were 45, 40, 35 and 30MPa and 55, 48.8, 42.7 and 36.6 MPa, respectively. Whereas the stress amplitudes and mean stresses for the wet tests were 25, 20, 15 and 10MPa, and 30.5, 24.4, 18.8 and 12.2 MPa, respectively. Fatigue tests were allowed to run until the specimen failed.

2.5.4 Viscoelastic Model for Dentin Adhesive

Perfectly elastic materials are modeled by spring elements, because they are deformed instantaneously when the load is applied. On the other hand, viscoelastic materials are modeled by combinations of springs and dashpots to describe their rate dependent behavior. In a Kelvin-Voigt model of viscoelastic solid, the spring and dashpot are connected in parallel. The force in this model is the sum of the forces in the dashpot and spring, while the displacement is the same in both the spring and dashpot. To model the mechanical behavior of our adhesive polymer, five Kelvin-Voigt elements with different retardation times were connected to form a Prony series [20]. The creep compliance function with five Kelvin-Voigt elements connected in series is given by the equation

$$J(t) = J_0 + J_1(1 - e^{-\frac{t}{\tau_1}}) + J_2(1 - e^{-\frac{t}{\tau_2}}) + J_3(1 - e^{-\frac{t}{\tau_3}}) + J_4(1 - e^{-\frac{t}{\tau_4}}) + J_5(1 - e^{-\frac{t}{\tau_5}}) \quad (2.1)$$

Here J_0, J_1, J_2, J_3, J_4 and J_5 are creep constants and τ_1, τ_2, τ_3, τ_4, τ_5 are the retardation times associated with each Kelvin-Voigt element. Using the creep compliance function, the creep constitutive equation is written as:

$$\varepsilon(t) = J(t)\sigma(0) + \int_0^t J(t-s)\frac{d\sigma(t)}{dt}ds \tag{2.2}$$

where σ (0) is the stress at the time zero. In a creep test constant stress is applied, therefore, $\frac{d\sigma(t)}{dt} = 0$, while in a static test stress is applied at a constant rate, that is $\frac{d\sigma(t)}{dt} = k$.

Aletrnatively, using the relaxation function, the constitutive equation is written as:

$$\sigma(t) = \int_{-\infty}^t G(t-s)\frac{d\varepsilon(t)}{dt}ds \tag{2.3}$$

where G(t) is the stress relaxation function is related to the creep compliance function, J(t), in the Laplace domain by the following relation: $G(s)J(s)=1/s^2$. In the time domain the relation between G(t)and J(t) is given as [21]

$$t = \int_0^t J(t-s)G(s)ds$$

The stress relaxation function for five Kelvin-Voigt elements connected in series is given by the equation

$$G(t) = G_0 + G_1(e^{-\frac{t}{\beta_1}}) + G_2(e^{-\frac{t}{\beta_2}}) + G_3(e^{-\frac{t}{\beta_3}}) + G_4(e^{-\frac{t}{\beta_4}}) + G_5(e^{-\frac{t}{\beta_5}}) \tag{2.4}$$

where β_0, β_1, β_2, β_3, β_4, β_5 are relaxation time which are related to retardation time τ_1, τ_2, τ_3, τ_4, τ_5. The stress relaxation function can be used to define the complex modulus of a viscoelastic material. Relaxation function in Eq. 2.4 can be rewritten in the following form:

$$G(t) = G(\infty) + \Delta G \tag{2.5}$$

And the complex modulus is given by

$$G(\omega) = G(\infty) + \omega\int_0^\infty \Delta G(s)[\sin(\omega s) + i\cos(\omega s)] \tag{2.6}$$

The complex modulus is separated into storage and loss modulus defined as follows

$$G(\omega) = G'(\omega) + iG''(\omega) \tag{2.7}$$

where G' is the storage modulus and G" is the loss modulus.

2.6 RESULTS

2.6.1 Degree of Conversion

Twelve randomly selected specimens were tested for degree of conversion after 5 days from the day of curing. The measured degree of conversion ranged between 90-92%.

2.6.2 Creep

Figures 2:5 and 2:6 give the results of the creep tests. While the creep behavior for the lower 3 stress-levels seems linear, the creep behavior at the highest stress-level appears to be nonlinear. For material to have linear creep behavior at different stress levels, strain ratio at any time should be equal to stress ratios. In the Figure 2:5, strain at 55MPa is approximately 1.8 times the strain at 30.5MPa at any time, which is equal to corresponding stress ratio. But this is not true for the 80MPa stress-level. In this case the strain ratio is not same as the corresponding stress ratio over the time of the test. Similarly in the Figure 2:6, using the same analysis as for the dry specimens, we can see that creep curves for the lower three amplitudes are approximately linear whereas 30.5MPa falls in the nonlinear range.

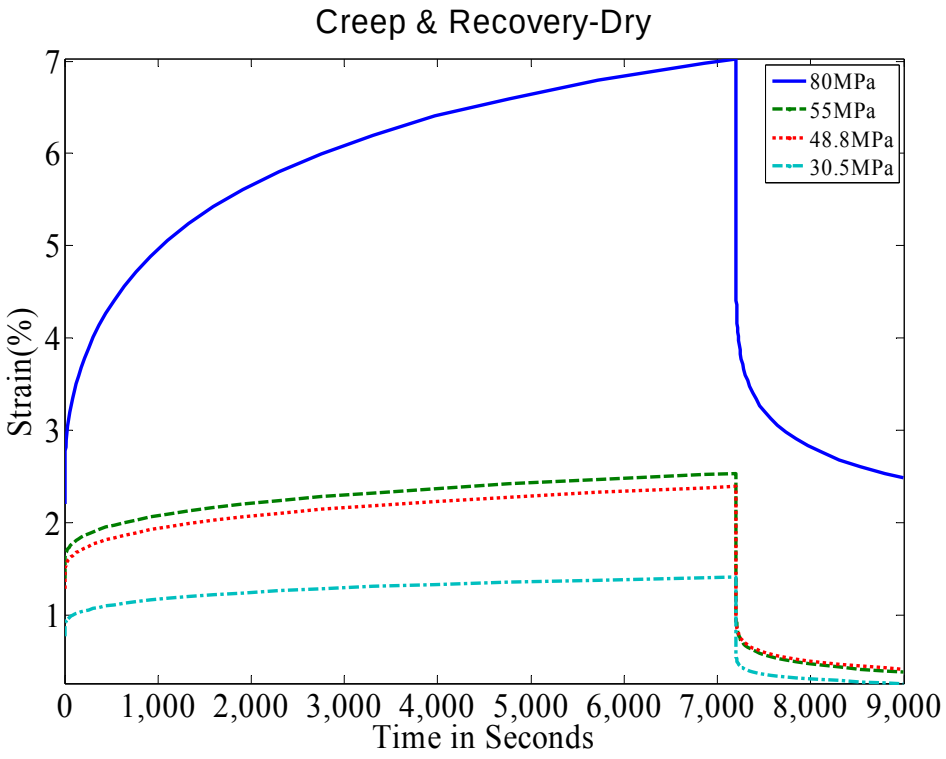

Figure 2:5 Creep and recovery test at different stress levels in dry conditions

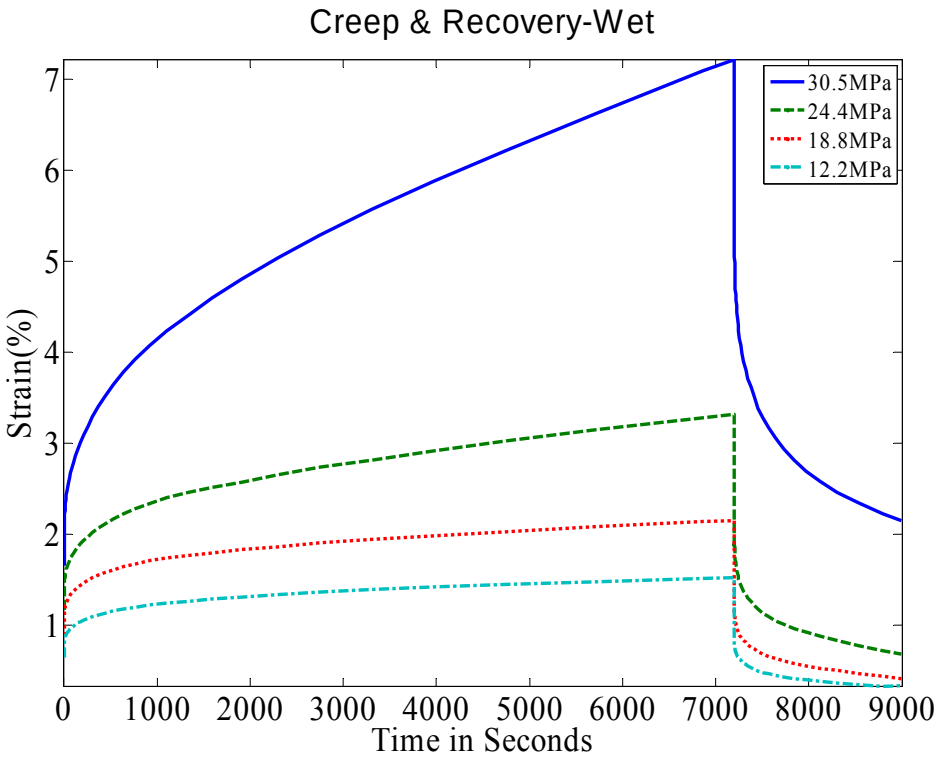

Figure 2:6 Creep and recovery test at different stress levels in wet conditions

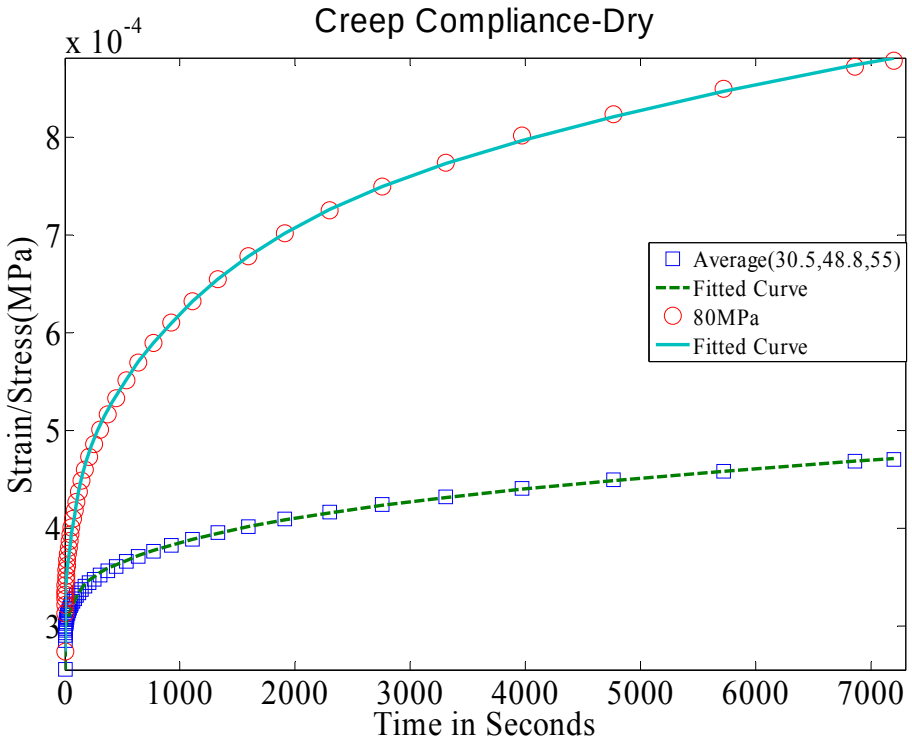

Figure 2:7 Creep compliance along with fitted curves for dry testing

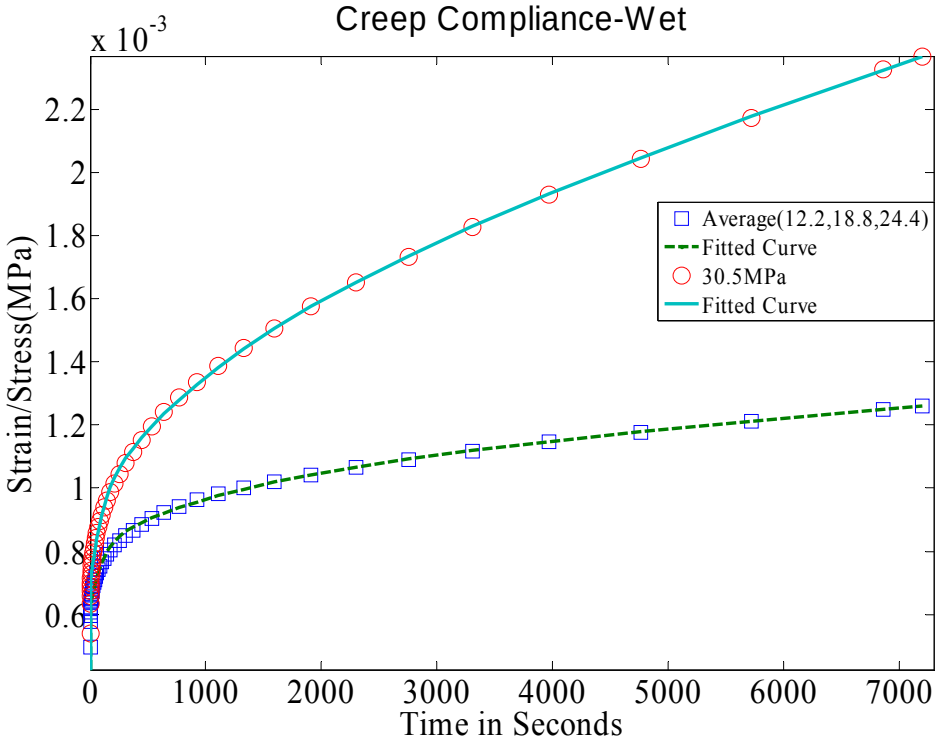

Figure 2:8 Creep compliance along with fitted curves for wet testing

The creep behavior shown in Figure 2:5 and 2:6, is modeled by fitting the data to the Prony series given in equation (2.1). This Prony series consists of 6 coefficients and 5 retardation times that need to be determined. To evaluate the constants, linear creep curves 30.5MPa, 48.8 MPa and 55 MPa in dry case and 12.2 MPa, 18.8 MPa and 24.4MPa in wet case were normalized with respect to applied stress and averaged to give one creep compliance curve each for wet and dry conditions as shown in Figure 2:7 and 2:8. We chose retardation times as listed in the Table 2-1 on trial and error basis to best fit the creep data. Thereafter creep compliance is fitted to Prony series using a non-linear least-square subroutine from Matlab 2006b. The calculated Prony series parameters are shown in Table 2-1 along with goodness of fit for both wet and dry conditions. While performing least-square fitting care was taken so that all creep constants are non-negative, because non-negative coefficients [22-23] lead to decrease of strain with time even when constant stress is maintained. There are many methods to avoid non-negative coefficients while fitting creep data like interactive adjustment of relaxation or retardation times [24], recursive algorithm [25] or power law presmoothing[26].

	Dry R^2=0.9958	Wet R^2=0.9912
J_0	2.55 10^{-10} m^2/N	4.25 10^{-10} m^2/N
J_1	4.20 10^{-11} m^2/N	1.97 10^{-10} m^2/N
J_2	4.16 10^{-11} m^2/N	1.90 10^{-10} m^2/N
J_3	4.96 10^{-11} m^2/N	1.64 10^{-10} m^2/N
J_4	1.41 10^{-11} m^2/N	3.80 10^{-10} m^2/N
J_5	1.5 10^{-10} m^2/N	1.27 10^{-9} m^2/N
τ_1	0.1sec	0.125 sec
τ_2	100 sec	100 sec
τ_3	1000 sec	1000 sec
τ_4	10000 sec	10000 sec
τ_5	100000 sec	100000sec

Table 2-1 Prony series parameters for creep compliance function.

2.6.3 Static Tests

Figures 2:9 and 2:10 give the stress-strain curves obtained from the static tests. As seen from these, figures, the loading rate has a large effect on the stress-strain behavior of dentin adhesives in both dry and wet conditions. As expected, the slopes of the linear part of the stress-strain curves, sometimes defined as the "elastic" modulus, are significantly different for the three loading rates. Table 2-2 and 2-3 compares the modulus from experiment and predicted using our viscoelastic model for three different loading. Predicted modulus was calculated based upon the slope of stress-strain curve predicted using the equation (2.2) when initial stress $\sigma(0)$ is zero and stress is applied at constant rate. Measured modulus is the elastic modulus (slope of linear portion) in Figure 2:9 and 2:10. Our prediction show close agreement with the moduli obtained from the measured curves, indicating that the five element Prony series is a reasonable model for the adhesive.

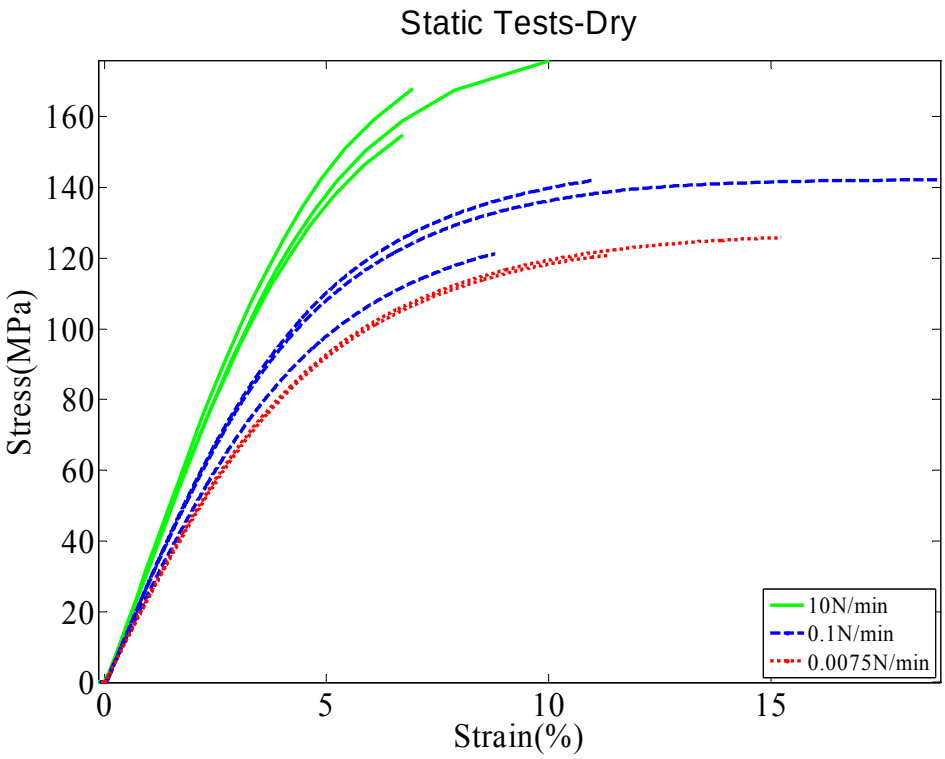

Figure 2:9 Stress -Strain curves at different loading rate in dry conditions.

Loading Rate	Measured Modulus(Dry)	Predicted Modulus(Dry)
10N/min	3.53 GPa	3.34 GPa
0.1N/min	3.06 GPa	2.93 GPa
0.0075N/min	2.56 GPa	2.42 GPa

Table 2-2 Elastic modulus in dry condition.

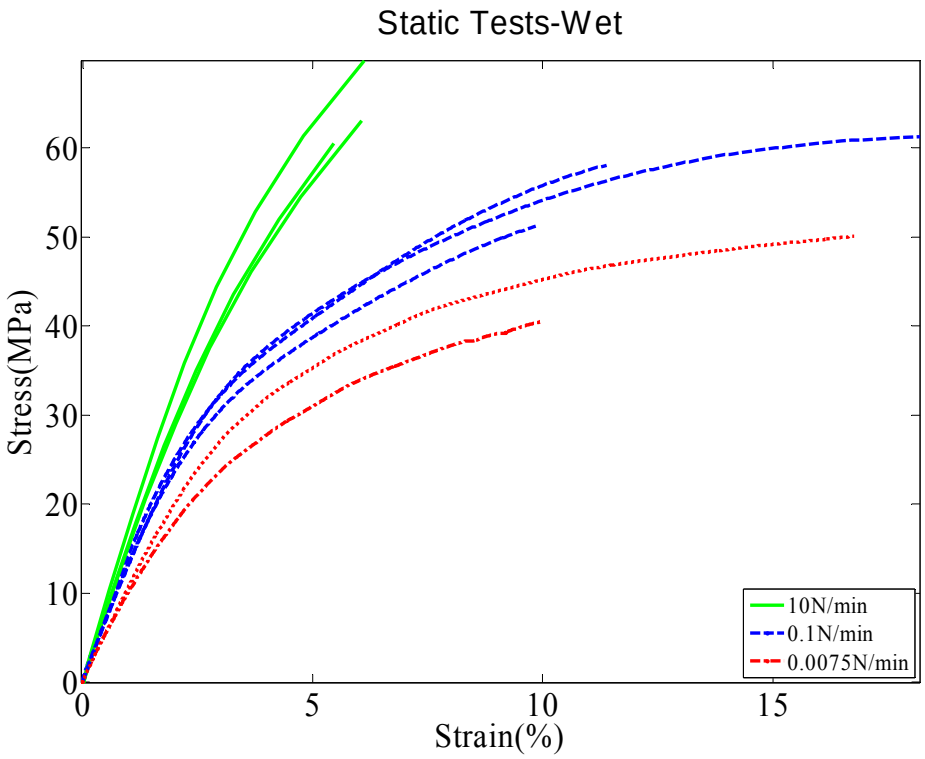

Figure 2:10 Stress-Strain curves at different loading rate in wet conditions

Loading Rate	Measured Modulus(Wet)	Predicted Modulus(Wet)
10N/min	1.62 GPa	1.59 GPa
0.1N/min	1.46 GPa	1.33 GPa
0.0075N/min	1.04 GPa	1.08 GPa

Table 2-3 Elastic modulus in wet condition

2.6.4 Fatigue Tests

Figures form 2:11 to 2:18 show the strain versus time curves for all the 4 stress amplitudes in both dry and wet fatigue tests. Each figure has measured curves from the experiment and a predicted curve calculated using equation (2.2), where $\sigma(t)=A\ sin(\omega t)$, A is the stress amplitude, $\omega=2f\pi$ and f is the cyclic frequency.. Fatigue tests were performed until the specimens reached failure. Stress amplitudes were different in wet conditions than in dry

because wet dentin adhesive samples have lower flexural strength then dry dentin adhesive samples as shown in Figure 2:10

Failure in a fatigue test occurs either (1) when the sample ruptures, or (2) when the strain in the sample becomes sufficiently large. Accordingly, our fatigue limit criterion is based upon the two failure modes: (1) when the sample is completely broken, (2) or when the strain in the sample has reached a specified limit. The value of limiting strain is chosen using the stress-strain curves from the static tests. From the stress-strain curves we can find the strain at which the material leaves the linear region and enters into the plastic state. For the case of dentin adhesives in this study the material enters the plastic state between 2.0% and 2.5%. Hence to show the effect of strain criteria on number of cycles to failure we have chosen 3 different strain values and have calculated the number of cycles to failure. Table 2-4 and 2-5 shows number of cycles to failure at different stress levels for dry and wet testing conditions.

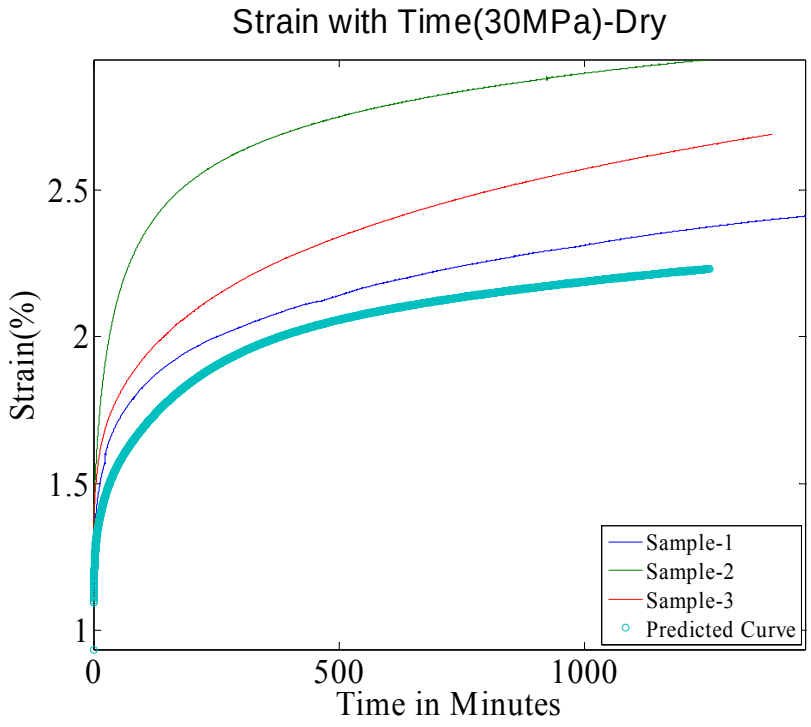

Figure 2:11 Strains versus time curves -Dry testing conditions-30MPa

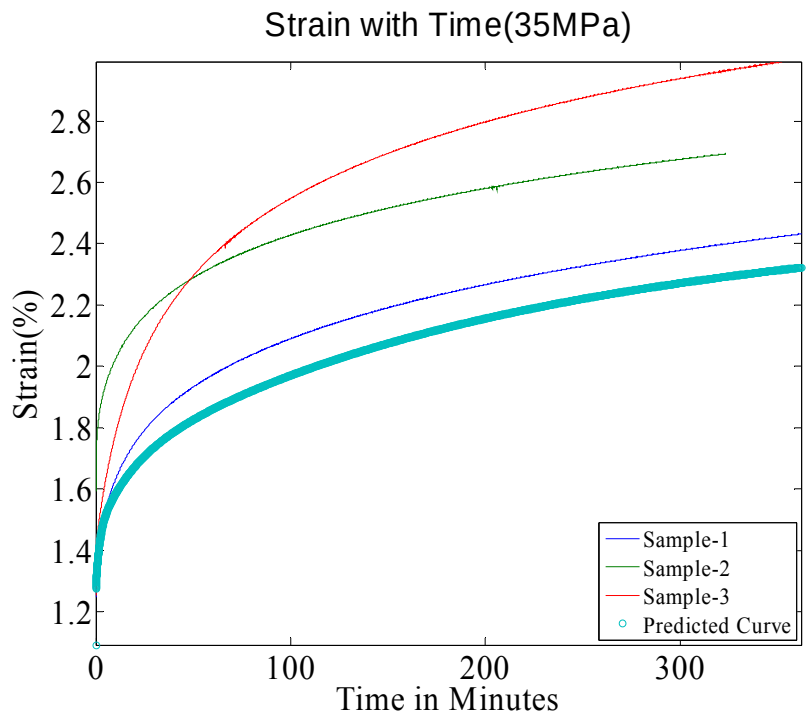

Figure 2:12 Strains versus time curves -Dry testing conditions-35MPa

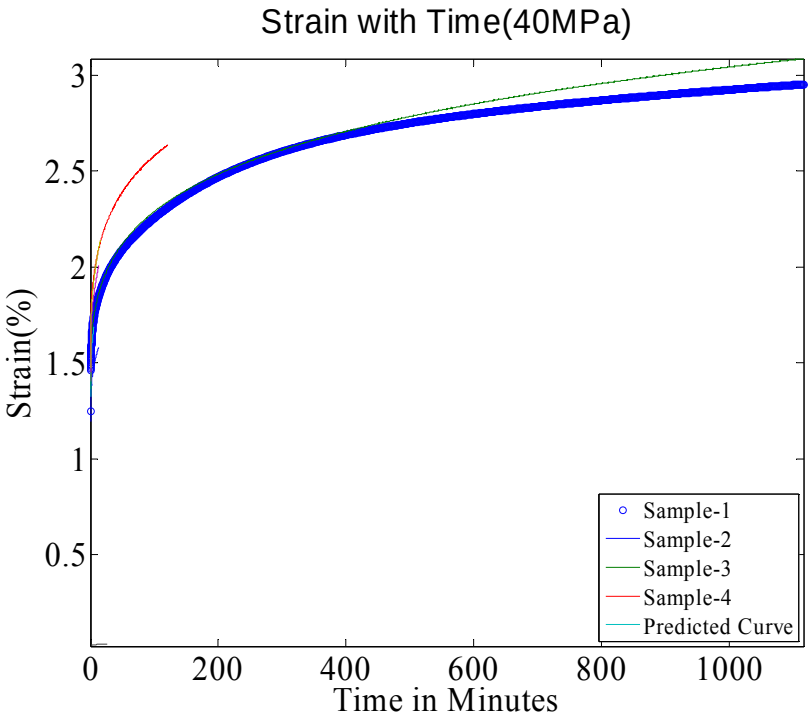

Figure 2:13 Strains versus time curves -Dry testing conditions-40MPa

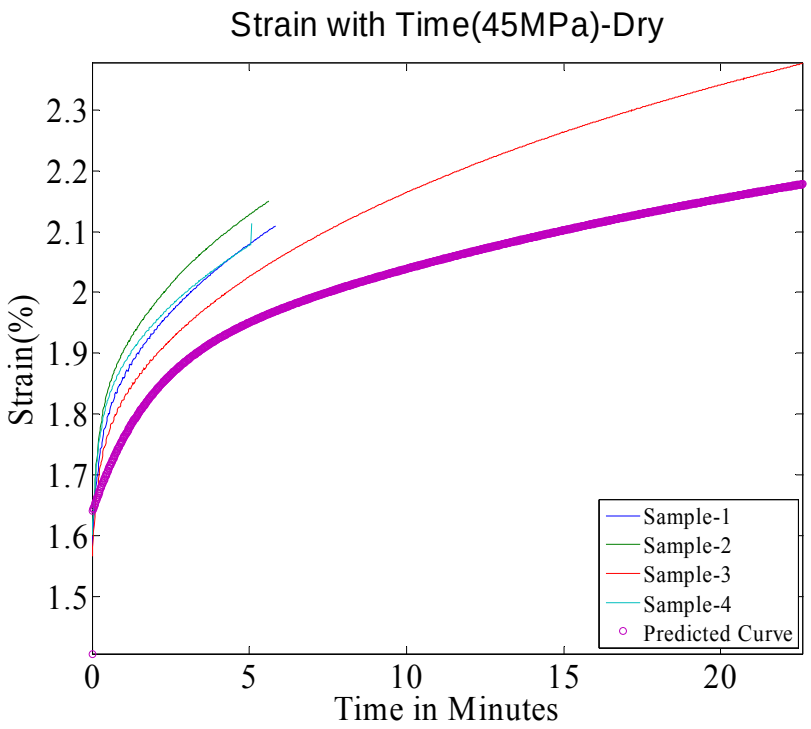

Figure 2:14 Strains versus time curves -Dry testing conditions-40MPa

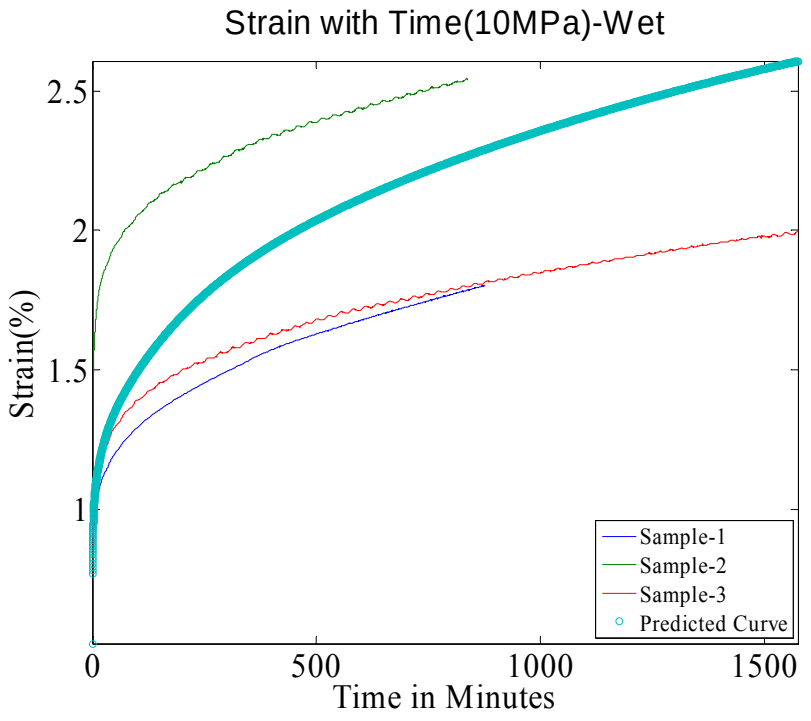

Figure 2:15 Strains versus time curves -Wet testing conditions-10MPa

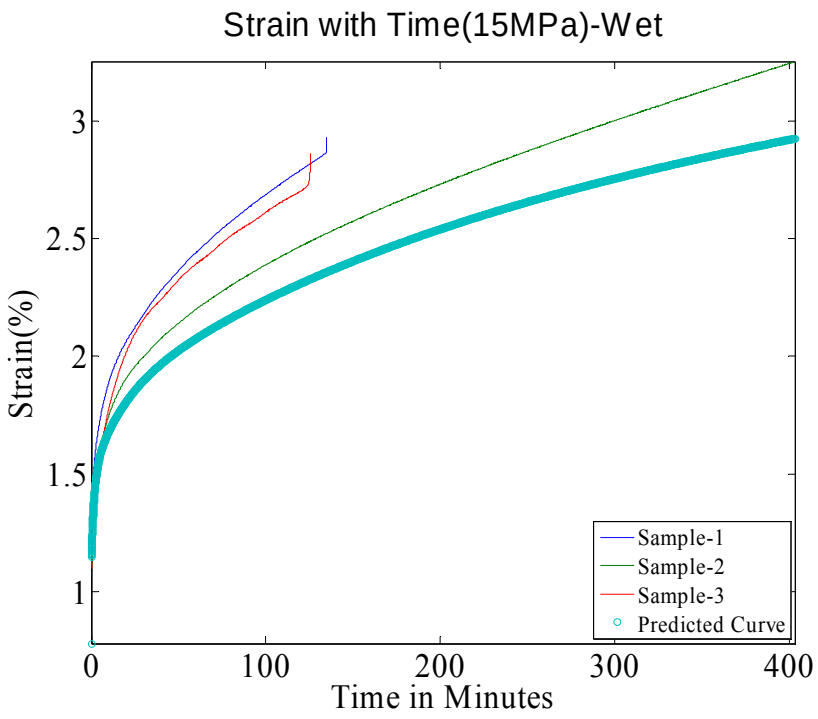

Figure 2:16 Strains versus time curves -Wet testing conditions-15MPa

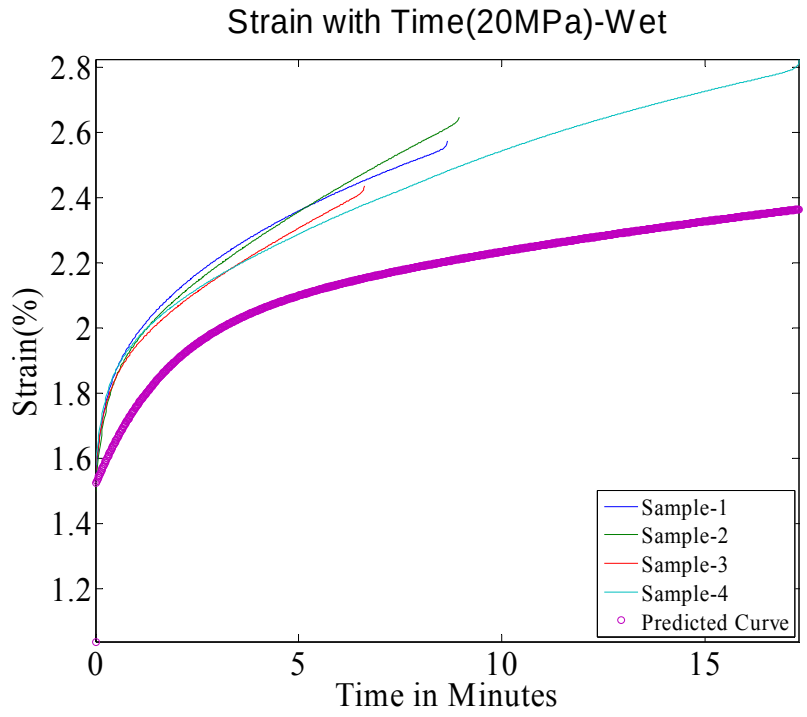

Figure 2:17 Strains versus time curves -Wet testing conditions-20MPa

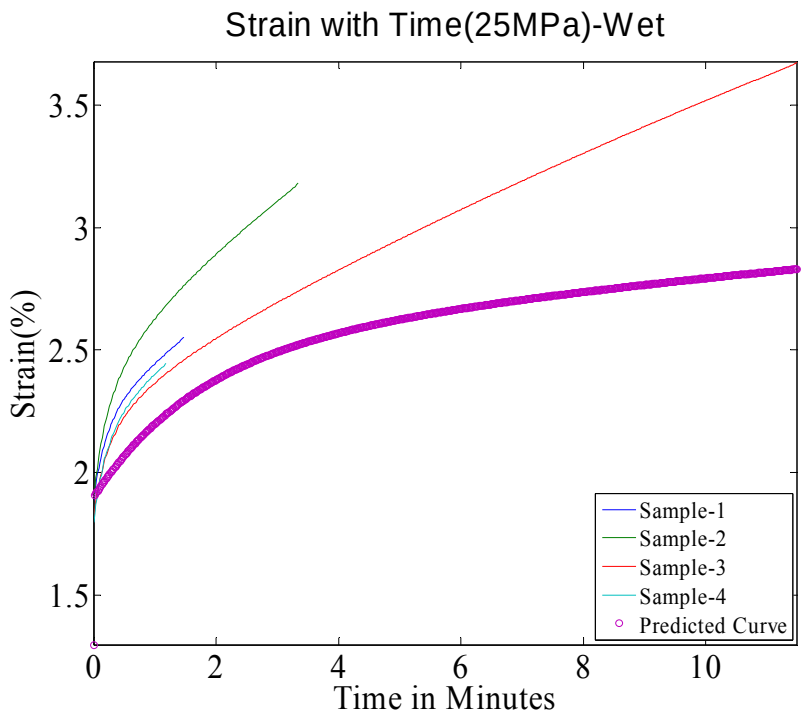

Figure 2:18 Strains versus time curves -Wet testing conditions-25MPa

2.6.4.1 Storage Modulus

While performing the fatigue tests, DMA saves the storage and loss moduli with time. By examining the storage and loss moduli curves we can determine if the material is softening or hardening with time. In the case of dry dentin adhesive polymers the storage modulus first decreases and then increases with time. These results suggest that there is softening of the material initially but the material hardens over time. Explanation of this phenomenon requires further investigation. Figures 2:19 and 2:20 reflect the variation of storage modulus with time for dry and wet testing respectively for all four different stress amplitudes.

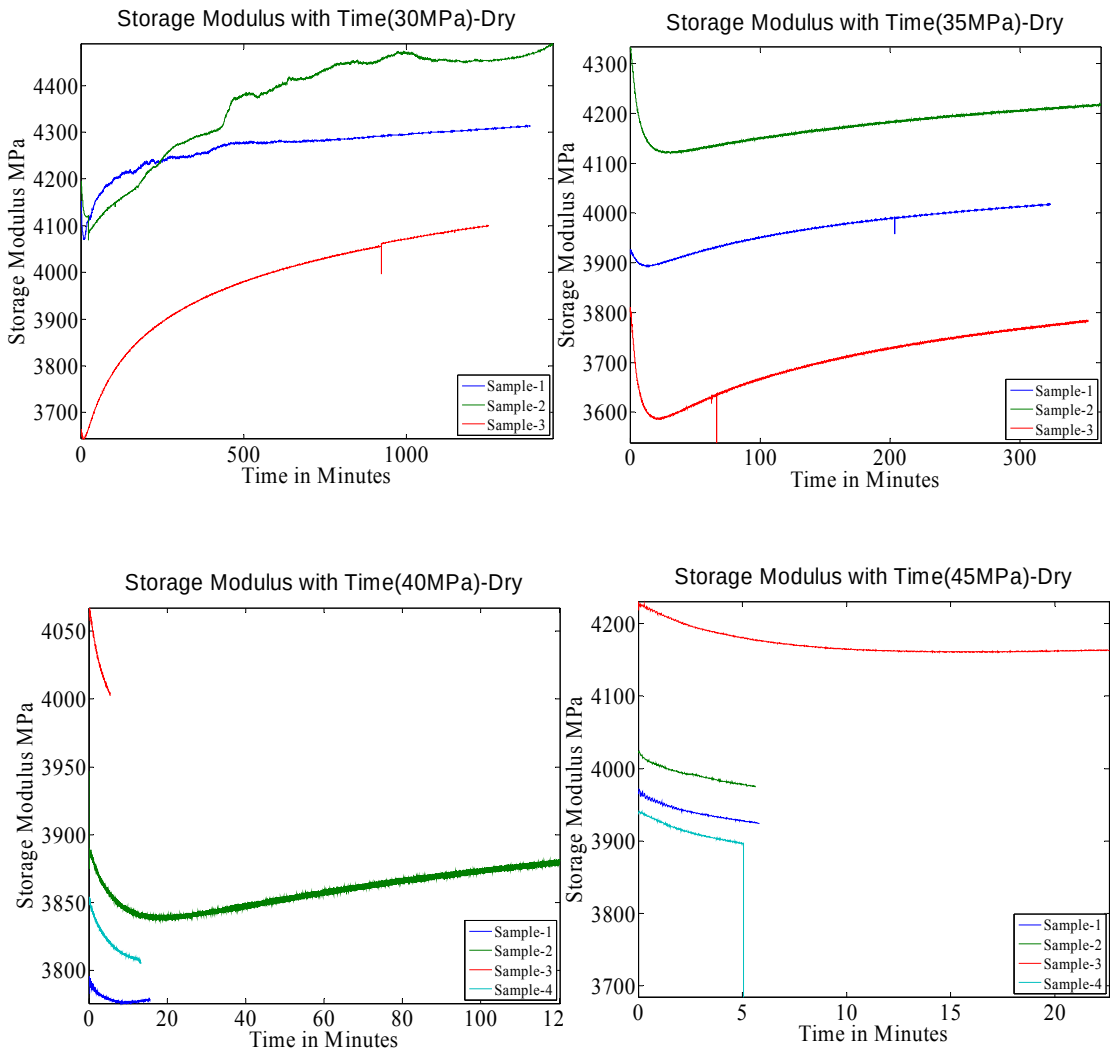

Figure 2:19 Storage moduli versus time-Dry testing

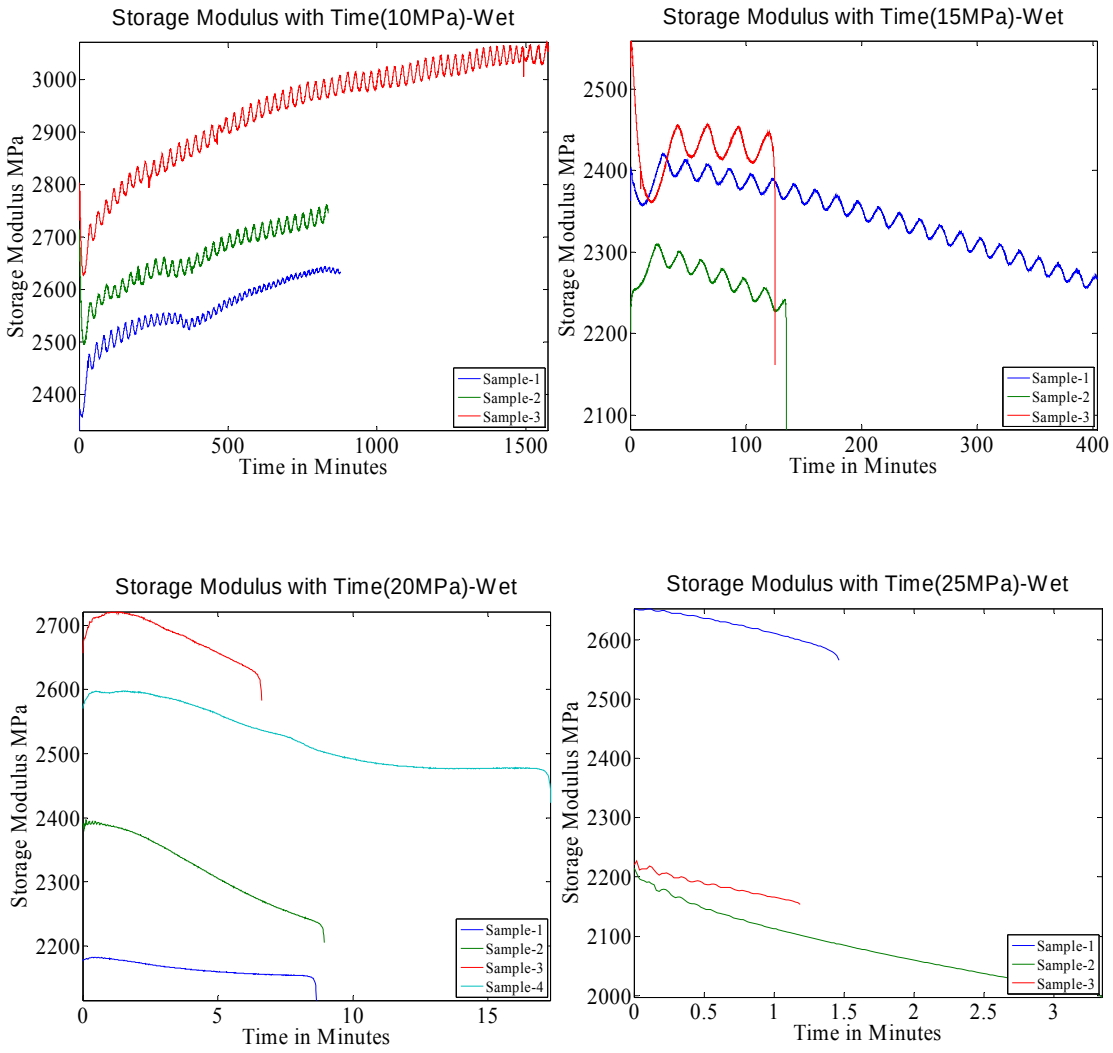

Figure 2:20 Storage moduli versus time-Wet testing

2.6.5 S-N Curve for Dental Adhesives

Using the failure criteria as described previously, the number of cycles to failure at particular stress amplitude for dry and wet conditions, respectively can be obtained as shown in Table 2-4 and Table 2-5. We have used three different values of strain to show how failure criteria affect the number of cycles to failure.

Stress Amplitude	No of Cycles 2.1% Strain Average (std)	No of Cycles 2.2% Strain Average (std)	No of Cycles 2.3% Strain Average (std)
45MPa	1679(402)	2113(926)	2529(1756)
40MPa	4275(721)	5382(1738)	6132(2865)
35MPa	15011(14233)	22478(20967)	33076(30284)
30MPa	67043(54877)	100581(85948)	147861(130737)

Table 2-4 Number of cycle to failure at different stress amplitude for dry testing

Stress Amplitude	No of Cycles 2.1% Strain Average (std)	No of Cycles 2.2% Strain Average (std)	No of Cycles 2.3% Strain Average (std)
25MPa	60(20)	100(33)	163(58)
20MPa	647(66)	985(107)	1387(153)
15MPa	7388(4574)	9995(6592)	13207(9033)
10MPa	258305(216769)	268116(202055)	279510(185455)

Table 2-5 Number of cycle to failure at different stress amplitude for wet testing

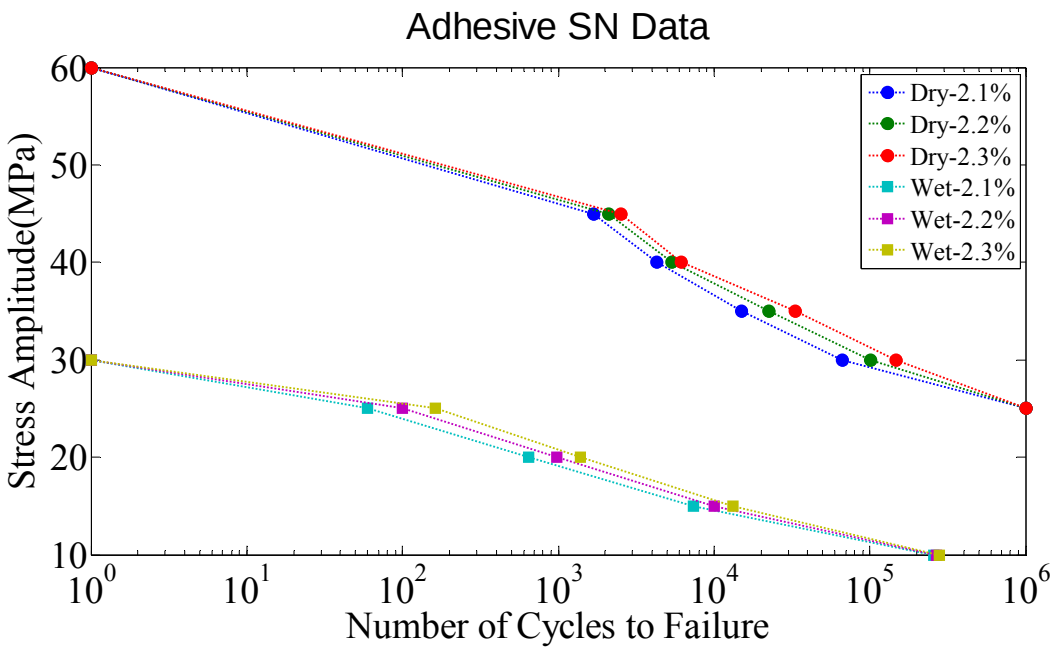

Figure 2:21 Measured SN data for dental adhesive in wet and dry conditions

Figure 2.21 gives a plot of the SN data calculated using the failure criterion as mentioned above. From this figure we can see that the dry dentin adhesives have much longer fatigue life as compared to wet adhesives. .

3.0 DENTIN-ADHESIVE INTERFACE FE MODEL

3.1 DENTIN MICRO-STRUCTURE

Dentin is a calcified tissue in human body and one of the four main components of the tooth. It is composed of 50% inorganic material (hydroxylapatite) and 30-35% organic materials like type I collagen [27] and 20% fluid by volume. At a micro-scale dentin structure is composed of dentinal tubules of very small diameter few microns surrounded by highly mineralized dentin called peritubular dentin [28]. Tubules run from pulp cavity to just below dentin enamel junction. These tubules are filled with pulp fluid in the healthy tooth. The density and size of tubules are not uniform throughout the tooth. Rather tubule size and density depends upon the location within the tooth. Near the dentin enamel junction the tubules have smaller size and less density, density and size increases as we reach pulp cavity and becomes largest close to the pulp chamber. Hence porosity of the dentin varies from 0 to 0.25 from dentin enamel junction to the pulp [29-30]. The tissue between two adjacent tubules is called intertubular dentin. Intertubular dentin is mainly composed of mineralized collagen fibrils; in healthy/sound dentin most of the collagen fibrils are perpendicular to the tubules.

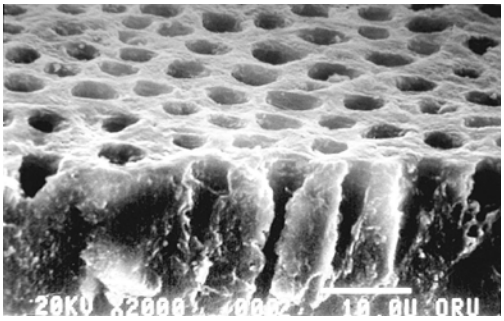

Figure 3:1 SEM image showing arrangement of tubules (Image from J David Eick)

3.1.1 Formation of Hybrid Layer

For composite tooth restorations, dentin is first etched using acidic agents which dissolve the calcium salts and form demineralized dentin. Demineralized dentin is composed of 30% type I collagen and 70% water. The hybrid layer (HL) is formed when the monomer mixture (adhesive resin) infiltrates the demineralized dentin matrix and the subjacent mineralized dentin. Formation of the hybrid layer depends upon the permeability of demineralized dentin and diffusibility of the applied adhesive resin. The hybrid layer has graded properties with depth as shown by previous investigators [31-33]. The thickness of the hybrid layer and amount of adhesive infiltration depends upon the type of adhesive used. In some cases the adhesive will not infiltrate to the depth of the demineralized dentin, an exposed collagen layer may exist below the hybrid layer [34].

3.2 COMPUTATIONAL UNIT CELL IDEALIZATION

Based upon the results from micro-Raman spectroscopic, scanning acoustic microscopic and optical microscopic investigations [32, 35-36], the dentin-adhesive (d/a) interface

may be represented as shown in Figure 3:2 [33]. .In Figure 3.2, the dentin-adhesive interface is considered to be composed of dental composite, the hybrid layer, the demineralized dentin, collagen, and adhesive. Based upon the organization of dentin-adhesive interface described above, a computational unit cell, which is representative of the interface section, is shown in the figure 3:2. A perfect square arrangement of tubules is assumed such that a three-dimensional parallelepiped unit cell with square cross-section may be used to represent the dentin-adhesive interface. To reduce the computation time the quarter symmetry is used in this study. The variation in micromechanical stresses are studied within this unit cell by considering a 3d model of this computational unit cell.

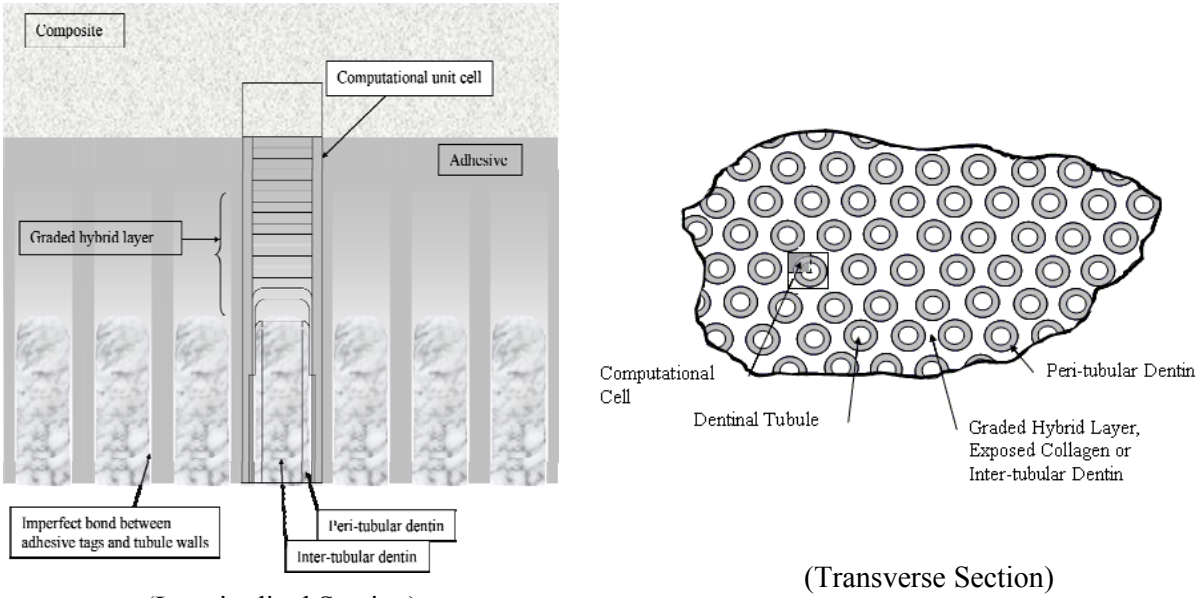

(Longitudinal Section)

(Transverse Section)

Figure 3:2 Idealized computational unit cell by Misra et al. [33]

3.3 FINITE ELEMENT MODEL OF D-A INTERFACE

To perform the micromechanical stress analysis on d-a interface along the longitudinal section, a three dimensional linear elastic Finite Element model of the above mentioned representative unit cell was developed.

The motivation for the 3d FE modeling using the representative computational unit cell was the 2d FE model developed by [33, 37] which showed stress concentrations in different material component along the longitudinal section. Since 3d models are more realistic compared to the 2d models, they are expected to give more accurate and reliable results which are close to actual conditions. Hence it is important to perform stress analysis on 3d dimensional model of computational unit cell.

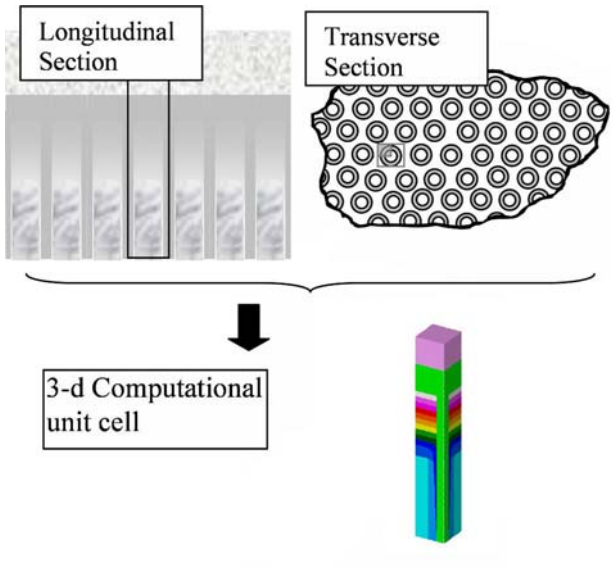

Figure 3:3 Schematic of idealized computational unit cell

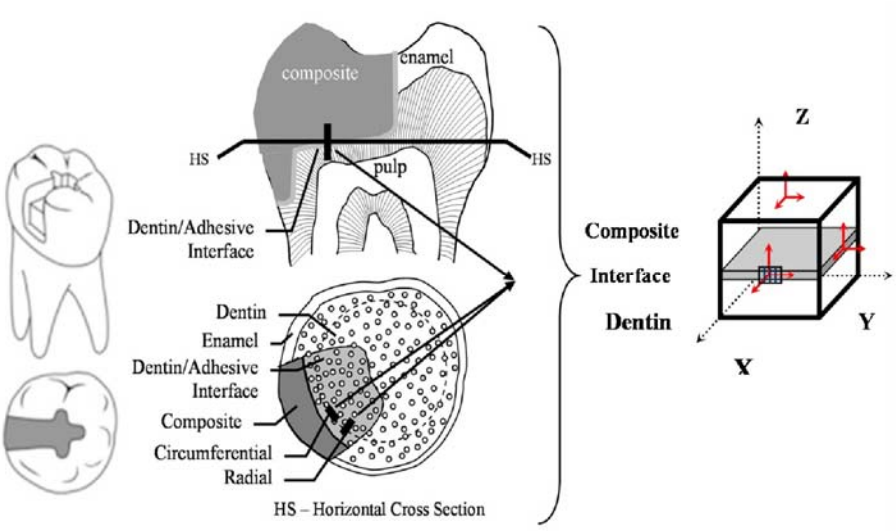

Figure 3:4 Schematic of d-a interface by misra et al. [33]

3.3.1 CAD Model and Geometry

The computational unit-cell depends on the geometrical properties of the d-a interface components. In our study dimension of unit cell is taken from the literature [33]. The unit cell was 37 μm high with a square cross-section of 8×8 μm. The unit cell is further divided in many different volumes to represent individual material component in the d-a interface as shown in Figure 3.5. The different material components considered are as follows: adhesive-collagen composite (hybrid layer), adhesive, composite, partially demineralized dentin, peritubular dentin and intertubular dentin. The adhesive appears as a layer underlying the composite as well as the adhesive tags formed as the adhesive flows into the dentinal tubules. Also, the adhesive-collagen composite (hybrid layer) is divided into several layers in order to represent the variation of properties within this material due to imperfect infiltration of adhesive into the demineralized dentin. To reduce the computation time quarter symmetry is exploited. The thickness of restorative dental composite is 5 μm; the adhesive layer is 5 μm. The thickness of partially demineralized dentin is 2.0 μm. The width of the peritubular

dentin varies and the height of the intertubular dentin is about 18 µm. The thickness of the hybrid layer in this study varied from 10 to 5 µm.

Real Units	Model Units
1 µm	10mm
1 N/mm	1/10 mN/mm
1 N/mm2	10-5 mN/mm2
1 MPa	10-5 mN/mm2
1 GPa	10-2 mN/mm2

Table 3-1 Scaling and unit conversion

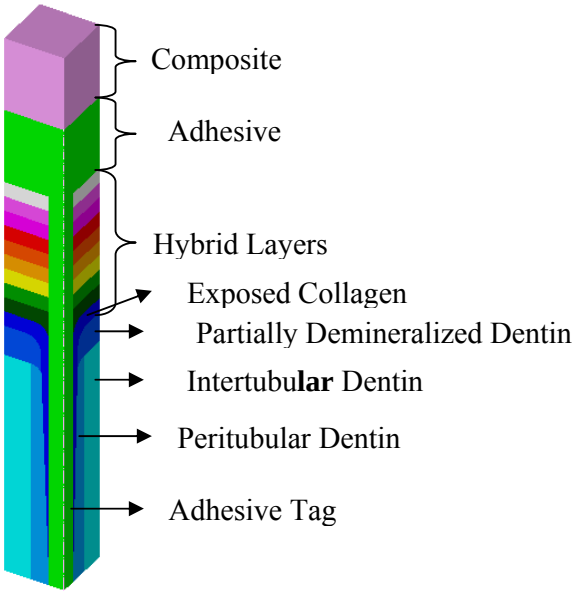

Figure 3:5 CAD model showing different material components.

3.3.2 Material Properties

We have assumed a linear elastic and isotropic behavior of the unit cell. The elastic properties for different phases in the unit cell are taken from literature [34, 38-39]. Elastic modulus of adhesive is taken 5GPa because at faster loading rates adhesive has higher modulus as shown in Table 2-2 (chapter 2). In our finite element calculation we simulate the

condition in which the load is applied at very fast rate hence elastic modulus of adhesive is taken to correspond to that for high loading rate.

S.No	Material	Elastic Modulus(GPa)	Poisson's Ratio
1	Composite	30	0.29
2	Adhesive	5	0.29
3	Peritubular Dentin	26	0.29
4	Intertubular Dentin	20	0.29
5	Partially Demineralized Dentin	13	0.29
6	Hybrid Layer-1	4	0.29
7	Hybrid Layer-2	3.75	0.29
8	Hybrid Layer-3	3.50	0.29
9	Hybrid Layer-4	3.25	0.29
10	Hybrid Layer-5	3	0.29
11	Hybrid Layer-6	2.75	0.29
12	Hybrid Layer-7	2.50	0.29
13	Hybrid Layer-8	2.25	0.29
14	Hybrid Layer-9	2	0.29
15	Hybrid Layer-10	1.75	0.45
16	GAP/Interface	0.01	0.29

Table 3-2 Material properties of different phases

3.3.3 Meshing

Free meshing is used to generate the mesh. This type of meshing is not constrained by the geometry hence we can mesh volumes with sharp edges and corners with minimum element distortion and better accuracy. In addition, convergence studies were performed to minimize the effect of element size. Different components in the 3d unit cell are meshed using 10 node parabolic tetrahedron elements; the size of the elements used for meshing depends upon the phase. Partially demineralized dentin and HL-10 were meshed with element size 0.1um, HL-1 to HL-9, composite, adhesive layer and intertubular dentin meshed with 0.5um and adhesive tag and peritubular dentin meshed with 0.25um element size. In the

final model, the total numbers of nodes were 575705 and total number of elements was 409345.

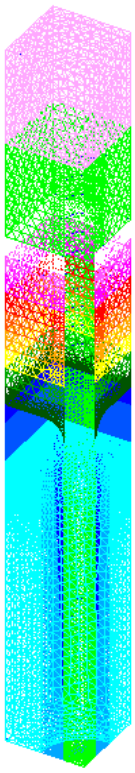

Figure 3:6 Finite element mesh of unit cell

3.3.4 Boundary Conditions

On the two symmetric sides as shown in Figure 3:7, we have symmetric boundary conditions and on the other two sides we have placed periodic boundary conditions. On the plane parallel to X axis, the out plane displacement (Y displacement) is zero, i.e. that unit cell is only allowed to deform in the XZ plane. Similarly on the plane parallel to Y axis displacement in the X direction is zero and unit cell is allowed to deform on YZ plane. The bottom of the unit cell is constrained in all three directions, i.e. zero displacement in x,y and z directions.

3.3.5 Type of Loading

In this study we have used two type of loading boundary conditions (1) stress controlled and (2) strain controlled. These loading conditions are considered for the following reasons; (1) actual boundary condition of the computational unit cell is not known (2) secondly in micromechanics boundary displacement or boundary tractions should produce equivalent overall constitutive parameters for the corresponding macro-element [40]. Hence to better understand the mechanical behavior of the unit cell under real conditions like chewing we have studied the behavior of unit cell under two types of loading conditions.

- **Stress Controlled:** In this approach a uniform tensile stress of 20 MPa is applied on the top surface of composite while the stresses in the other phases are calculated.
- **Strain controlled**: In this approach a unit strain is applied on the top of composite. Data surface is used here to apply a linear strain on the boundaries of the unit cell.

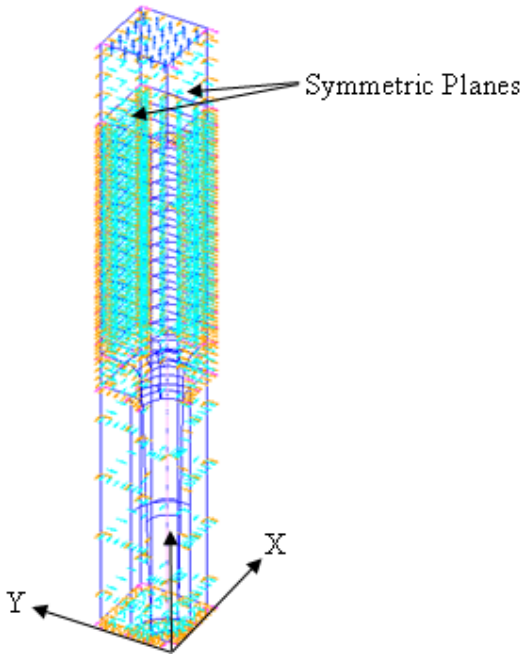

Figure 3:7 Loading and boundary conditions on unit cell

3.4 PARAMETRIC STUDY

Further, parametric studies are performed on the computational unit cell to show the effect of change of physical characteristics of dentin-adhesive interface, like thickness of hybrid layer, material properties of hybrid layer and so forth. In the current study to show the variation in microstructure of d-a inter we have developed five different models.

- **Model 1:** *Graded Hybrid Layer*- When hybrid layer has uniformly decreasing elastic modulus of along its depth.
- **Model 2:** *Uniform Hybrid Layer*- Due to etching profile hybrid layer formed could have uniform properties throughout the depth
- **Model 3:** *Unit cell with short Hybrid layer*- In some cases hybrid layer can be short hence a unit cell with 5µm graded hybrid layer is developed
- **Model 4:** *Unit Cell with no Partially Demineralized Dentin*-Due to the nature of etching, there is no zone of partially de-mineralized dentin in computational unit cell.
- **Model 5:** *Unit cell with a spherical defect in uniform hybrid Layer*. Due to phase separation in adhesive because of water some cavities or defects could form in the adhesive. These defects could be present anywhere in the d-a interface. The condition would be worse if cavities are formed in the adhesive tag. Hence we developed a model with quarter spherical cavity of 0.8 micrometer diameter in the adhesive tag. The hybrid layer in this model has uniform properties throughout.

Parametric studies were performed for both stress and strain loading conditions. But effect of spherical cavity is studied in stress controlled case only. Total 9 parametric models were developed, 5 models for stress controlled case and 4 models for strain controlled case.

3.5 RESULTS

For all the models maximum principle stress was studied. Stress distribution was studied for the complete unit cell along with individual material components like adhesive tag, exposed collagen, peritubular dentin, and intertubular dentin.

3.5.1 Stress Controlled

Figure 3:8 shows the maximum principle stresses in the four different models under the stress controlled loading. High stresses, approximately 1.5 times of that applied, can be seen in the adhesive tags (Figure 3:9) because of softer material properties and geometry of adhesive tags. But, stress distribution and stress values differ from model to model. Stresses in the composite, adhesive layers and intertubular dentin were fairly uniform and almost equal to that applied. Peritubular dentin is also experiencing high stress but not as high in adhesive tags. Most of the stresses seen in unit cells were tensile with very little compressive stresses.

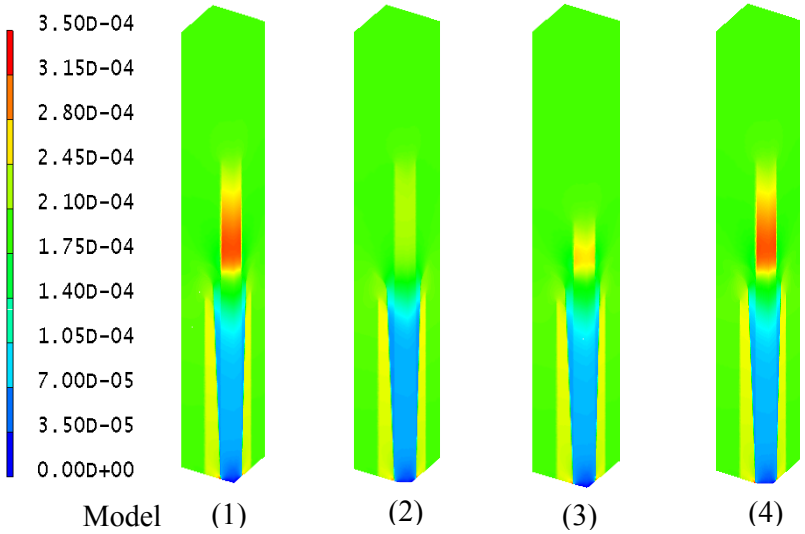

Figure 3:8 Maximum principle stress ($\times 10^5$MPa) in unit cell-Stress controlled (1) Graded HL (2) Uniform HL (3) Short HL (4) No partially demineralized dentin

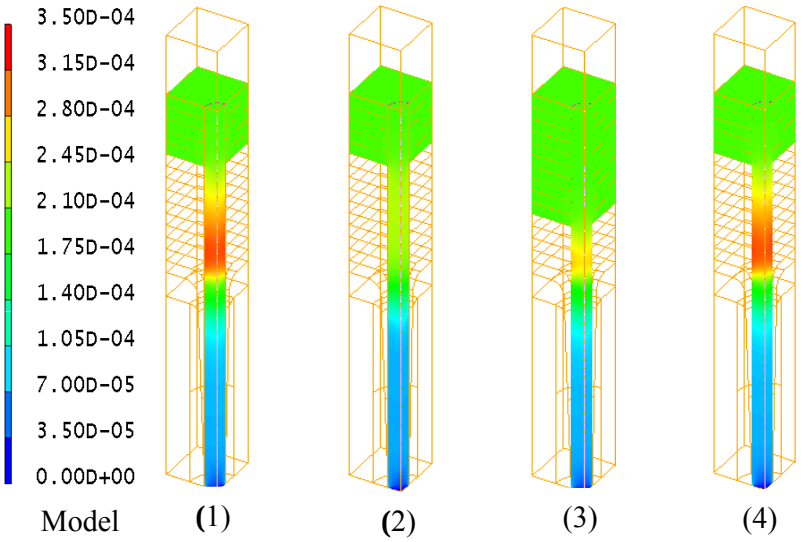

Figure 3:9 Maximum principle stress ($\times 10^5$MPa) in adhesive tag -Stress controlled (1) Graded HL (2) Uniform HL (3) Short HL (4) No partially demineralized dentin

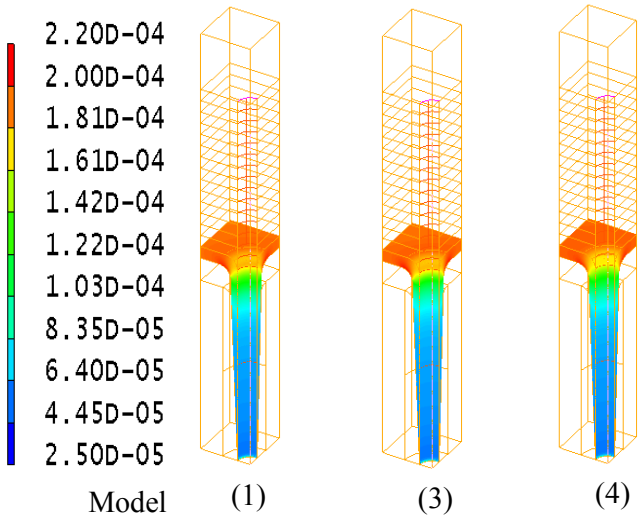

Figure 3:10 Maximum principle stress ($\times 10^5$MPa) in exposed collagen-Stress controlled (1) Graded HL (3) Short HL (4) No partially demineralized dentin

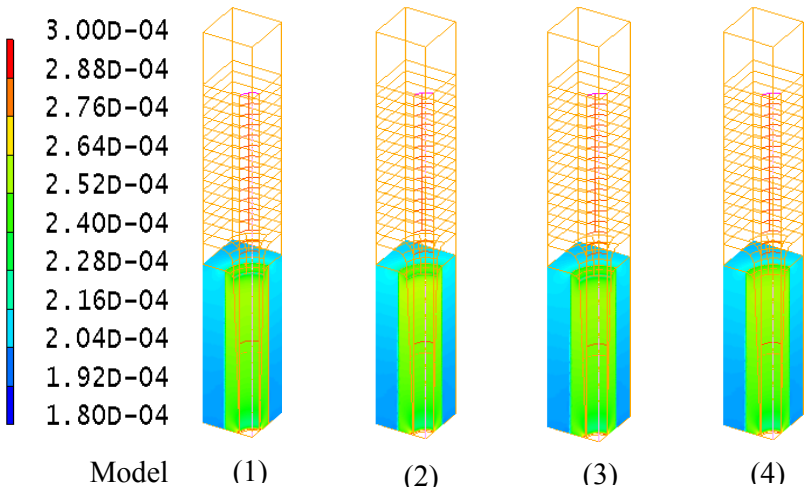

Figure 3:11 Maximum principle stress ($\times 10^5$MPa) in peritubular & intertubular dentin-Stress controlled (1) Graded HL (2) Uniform HL (3) Short HL (4) No partially demineralized dentin

3.5.2 Hybrid Layer with a defect

If we compare unit cell with uniform hybrid layer with unit cell with a spherical cavity in the adhesive tag as shown in Figure 3:12 and 3:13, we notice that the overall stresses are higher because of the presence of the defect. In the vicinity of the cavity stress is very high, approximately 2.25 times which could initiate the failure in the adhesive tag. But the effect of the spherical defect is highly localized i.e. stress decreases very rapidly as we move away from the cavity and it does not effect stress distribution in the overall model. Hence the location and size of the cavity can have a large impact on the stress distribution.

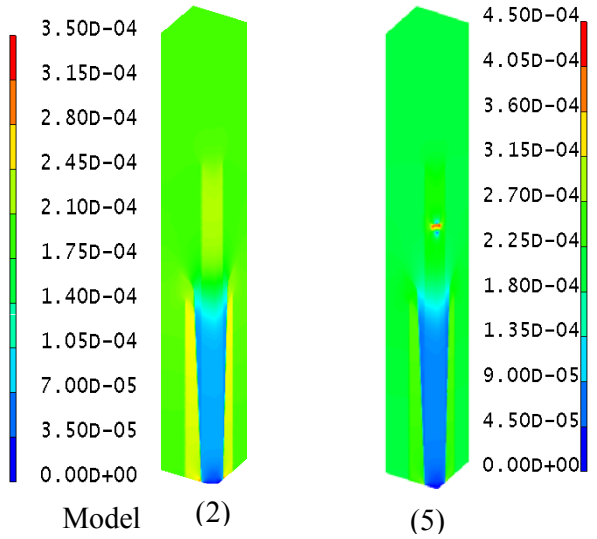

Figure 3:12 Maximum principle stress ($\times 10^5$MPa) in unit cell-Stress controlled (2) Uniform HL (5) Uniform HL with cavity.

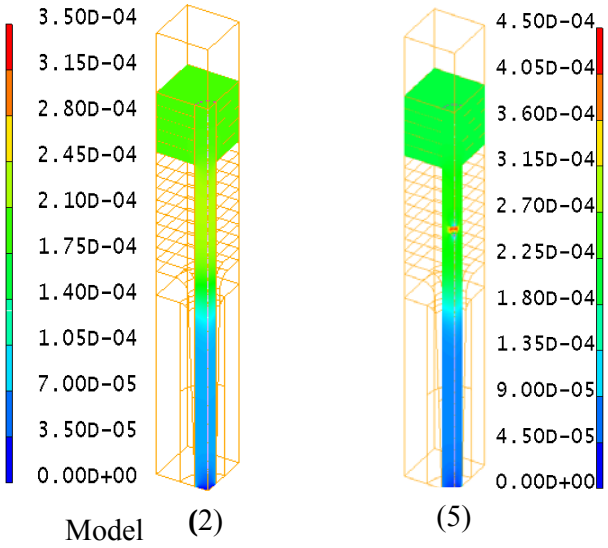

Figure 3:13 Maximum principle stress ($\times 10^5$MPa) in adhesive-Stress controlled (2) Uniform HL (5) Uniform HL with cavity.

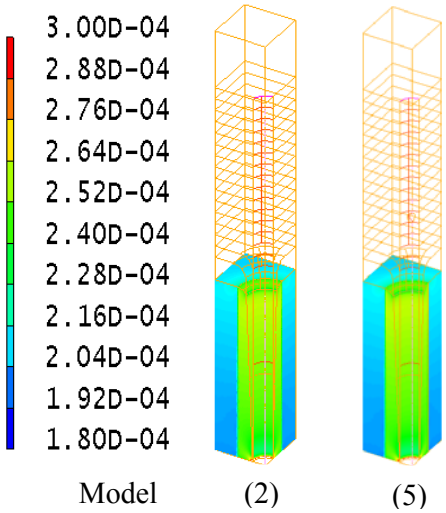

Figure 3:14 Maximum principle stress intertubular & peritubular-Defect in adhesive tag

3.5.3 Strain Controlled

Figure 3:15 is showing the maximum principle stress in computational under uniform strain controlled loading. Because of the boundary conditions the stresses in the adhesive and adhesive tags are less as compared to stresses in dentin and composite. Hence in this case adhesive and adhesive tags are experiencing stress shielding due to the nature of boundary condition. Unit cells with uniform hybrid layer and short hybrid layer are having lower stresses in adhesive tags as compared to graded hybrid layer as shown in Figure 3:16 and 3:17

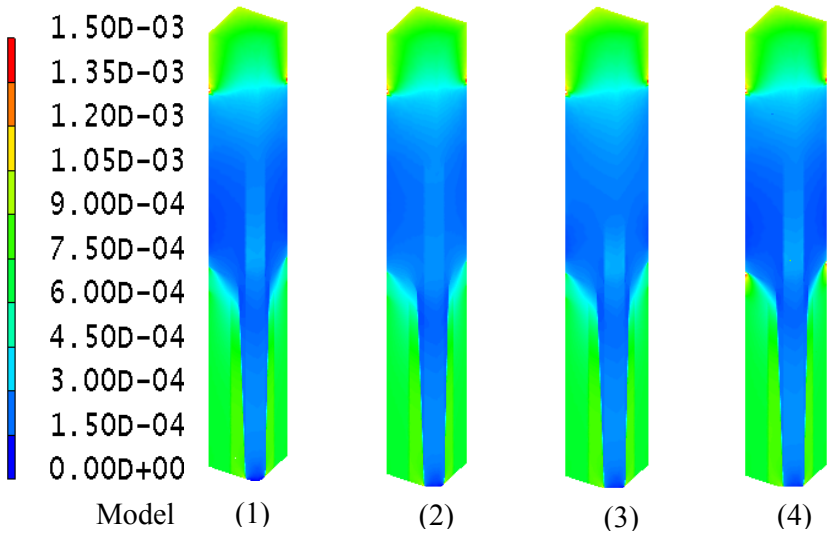

Figure 3:15 Maximum principle stress ($\times 10^5$MPa) in unit cell -Strain controlled (1) Graded HL (2) Uniform HL (3) Short HL (4) No partially demineralized dentin

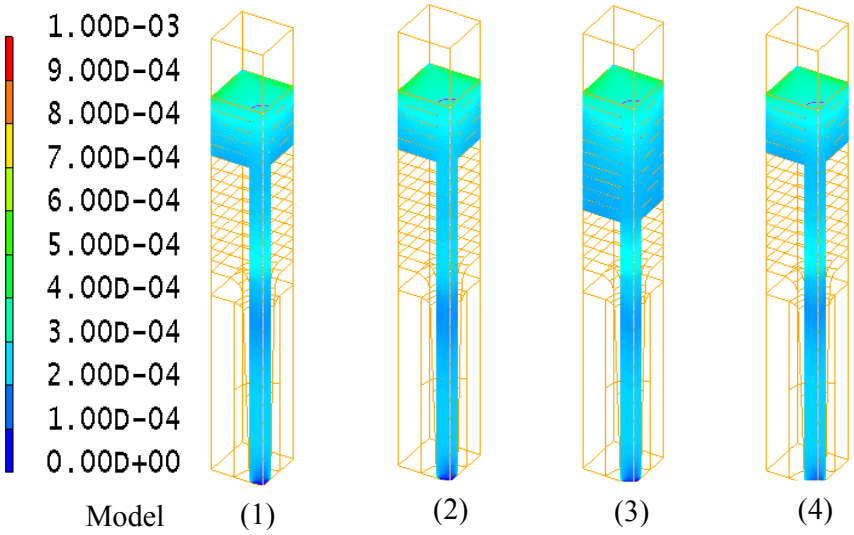

Figure 3:16 Maximum principle stress ($\times 10^5$MPa) in adhesive tag -Strain controlled (1) Graded HL (2) Uniform HL (3) Short HL (4) No partially demineralized dentin

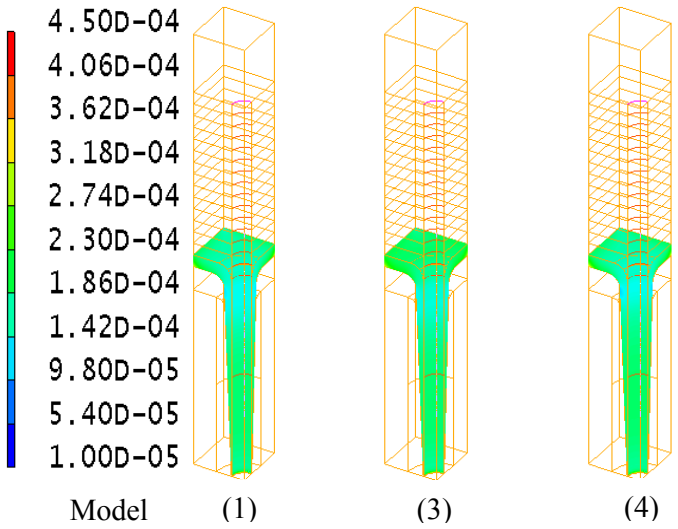

Figure 3:17 Maximum principle stress ($\times 10^5$MPa) in exposed collagen -Strain controlled (1) Graded HL (2) Uniform HL (3) Short HL (4) No partially demineralized dentin

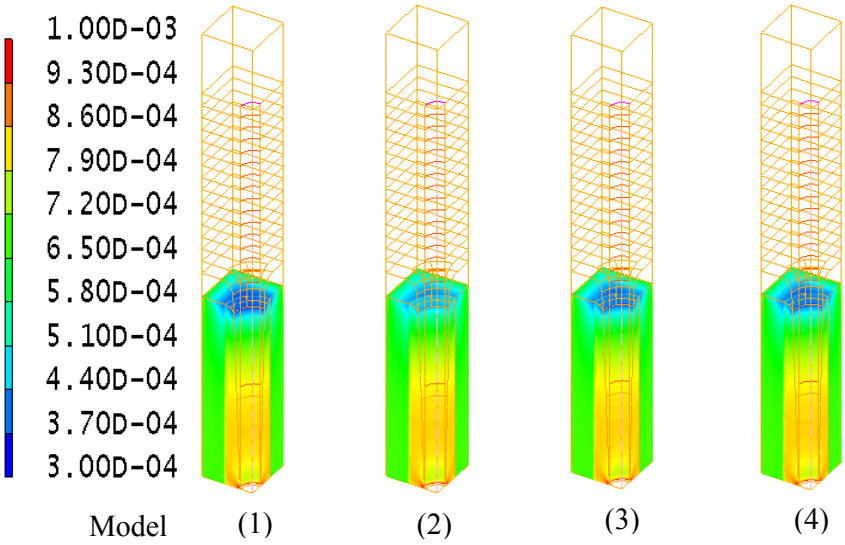

Figure 3:18 Maximum principle stress ($\times 10^5$MPa) in intertubular & peritubular dentin-Strain controlled (1) Graded HL (2) Uniform HL (3) Short HL (4) No partially demineralized dentin

3.6 CALCULATION OF STRESS CONCENTRATION FACTORS

Stress concentration factor is defined as the ratio of highest stress experienced by the individual material components divided by the global stress which is applied on the d-a interface. Calculation of stress concentration was important to predict the fatigue life of the dentin adhesive interface under cyclic loading. For example, in the case where 20 MPa tensile stress is applied on the top surface of the composite because of stress concentration some material components could experience stress higher then 35 MPa. To calculate the stress concentration factor, top 5% of high stress experiencing elements of the particular component were selected and averaged. Then 2 sigma standard deviation criteria were used to select elements among those 5% selected, so we can discard high stress elements because of geometry artifacts. Then these 2 sigma selected elements were again averaged to give peak stress in those particular material components. If the concentration factor is denoted by f, then f = average high stress in the material component/global stress applied on the composite top surface.

For the stress controlled case global stress was 20 MPa and for the strain controlled case stress on the top surface of composite was averaged which was 84MPa. Stress concentration factor for stress and strain controlled case is shown in Table 3-3 and 3-4

Phase	Graded HL	Uniform HL	Short HL	No Partially Demineralized Dentin
Adhesive	1.50	1.16	1.17	1.50
Exposed Collagen	1.04	N/A	1.04	1.05
Partially Demineralized Dentin	1.18	1.18	1.16	N/A
Dentin(Intertubular & Peritubular)	1.30	1.30	1.30	1.30

Table 3-3 Stress concentration factor-Stress controlled

Phase	Graded HL	Uniform HL	Short HL	No Partially Demineralized Dentin
Adhesive	0.338	0.334	0.341	0.34
Exposed Collagen	0.30	N/A	0.0.31	0.31
Partially Demineralized Dentin	0.688	0.731	0.72	N/A
Dentin(Intertubular & Peritubular)	1.042	1.042	1.06	1.42

Table 3-4 Stress concentration factor-Strain controlled

4.0 DENTIN-ADHESIVE FATIGUE LIFE PREDICTION

For fatigue life prediction of the dentin-adhesive interface, the stress that developed in the different material components of the d-a interface in the finite element model were used against S-N (stress-cycle) curves corresponding to each component of the d-a interface. When a global stress is applied on the computational unit cell of the d-a interface, different components of the d-a interface experience different maximum stresses. For example, the stress concentration in the adhesive tags varied from ~1.2 to 1.5 times the applied load depending upon the hybrid layer properties. The overall fatigue life of the d-a interface is governed by the fatigue life of the component with the shortest fatigue life at the local level. Thus by using S-N curves for different components and combining them with the stresses from linear elastic FE models (chapter 4), we can estimate the overall fatigue life of the d-a interface.

4.1 S-N CURVES

For the reliability of this approach it is critical to have correct S-N curves for different phases of d-a interface. In the current study due to lack of data and to demonstrate the methodology we have used just three phases, dentin, exposed collagen and adhesive. S-N curve for dentin is taken from literature [8-9]. The data is sampled at frequency of 2, 10 and 20 Hz. The stress ratio was 0.1 for all the tests. Figure 4:1 shows the SN data for the human

dentin. Exposed collagen data were also taken from the literature [7]. Authors have performed fatigue tests on type I collagen fibers from wallaby tail tendons. Figure 4:2 shows the S-N data for exposed collagen. Adhesive S-N data shown in Figure 4:3 were taken from the experiments performed in the current study as described in chapter 2. Currently we have used the S-N data for adhesive in dry conditions only. All the testing was performed at stress ratio R=0.1 and frequency of 5Hz.

The SN data for all the three phases dentin, exposed collagen and adhesive are further fitted with a power law given by the following formula $\sigma_a = A(N_f)^B$ Where A and B are fitting constants. Least square subroutine from Matlab is used to fit the S-N data and determine fitting constants A and B.

Fitting Constants	Exposed Collagen	Dentin	Adhesive
A	51.624	101.830	61.682
B	-0.105	-0.073	-0.056
R^2	0.67	0.71	0.90

Table 4-1 Fitting Constants

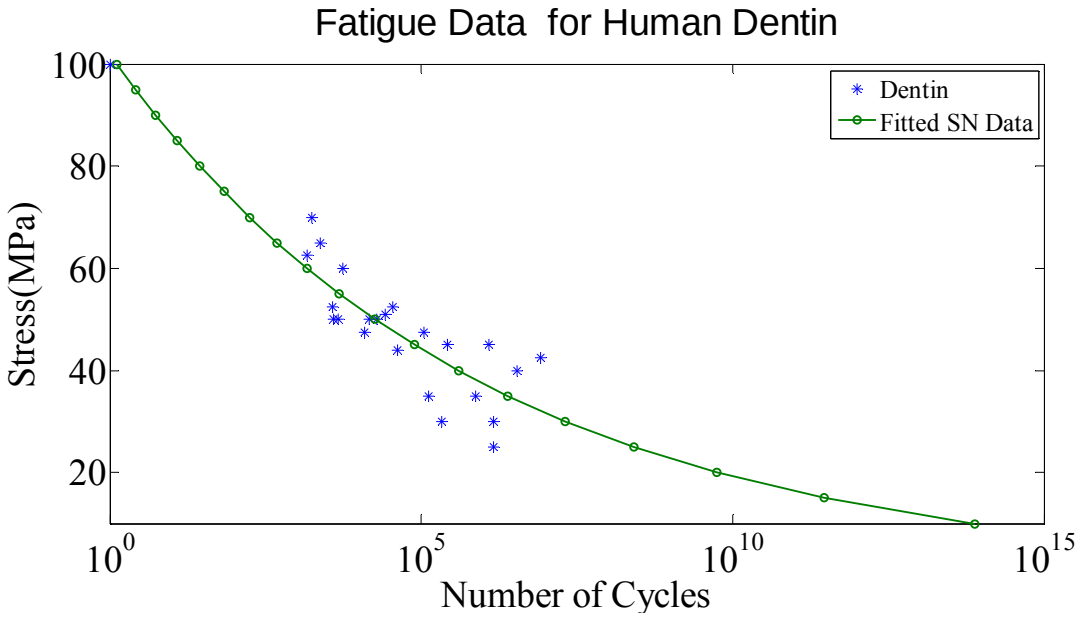

Figure 4:1 Measured SN data for dentin [9]

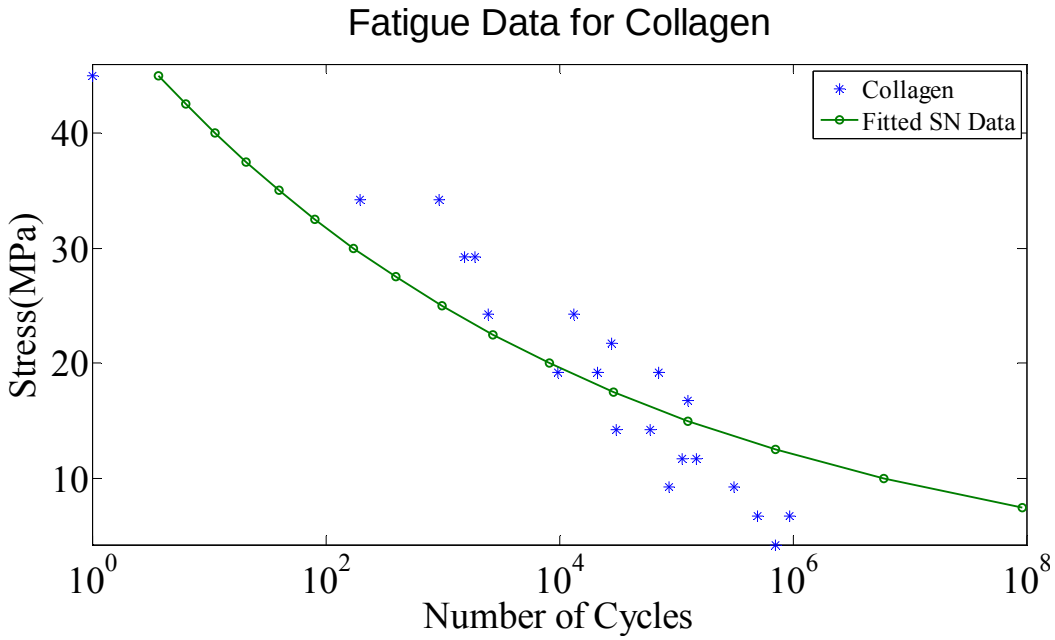

Figure 4:2 Measured SN data for collagen [7]

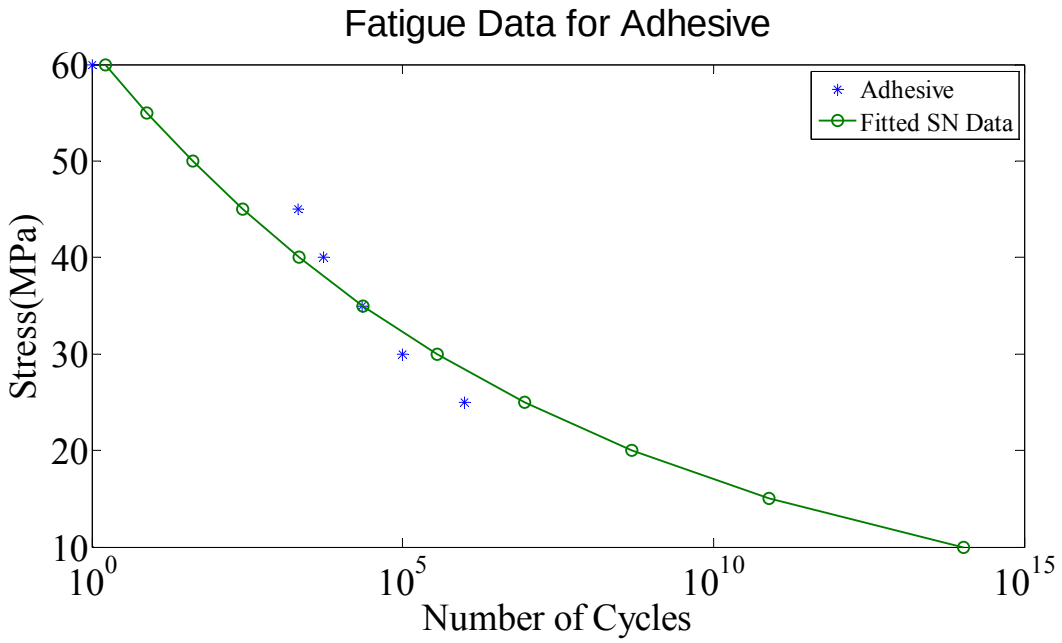

Figure 4:3 Measured SN data for adhesive

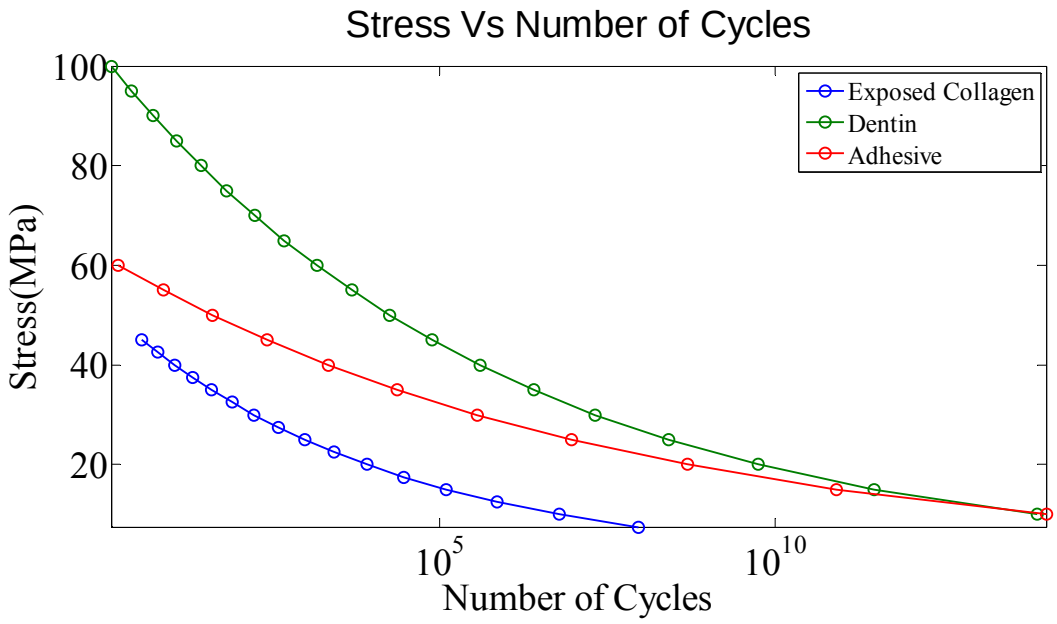

Figure 4:4 Fitted SN data using power law

4.2 MASTER SN CURVE CALCULATION

To obtain the master SN curve for the d-a interface, we compute the local stress-level under different global stresses utilizing the stress concentration factors developed in section 3.6. The local stresses are defined as follows:

$$\sigma_l = \sigma_g f \tag{4.1}$$

where f is stress concentration factor and σ_g is the global stress. In addition, we first need to establish the strength and the endurance limit of the d-a interface as these determine the maximum and minimum stress amplitude over which the S-N curves needs to be established. Strength is defined as stress at which material will last only for 1 cycle under constant amplitude stress loading. Strength of different phases at global level in both strain and stress controlled model is given in Table 4-2. Endurance limit is defined as the stress amplitude at which material will not fail under constant amplitude cyclic stress loading for certain number

of cycles. The number of cycles in our methodology is taken to be 10^6. The endurance limits are tabulated in Table 4-3.

Phase	Stress Controlled		Strain Controlled	
	Graded HL	Uniform HL	Graded HL	Uniform HL
Dentin	78.33	78.33	97.72	97.72
Adhesive	41.12	53.17	154.20	205.60
Exposed Collagen	49.63	N/A	161.32	N/A

Table 4-2 Strength for each phase at global level

Phase	Stress Controlled		Strain Controlled	
	Graded HL	Uniform HL	Graded HL	Uniform HL
Dentin	28.76	28.76	35.96	35.96
Adhesive	18.90	24.42	83.83	84.84
Exposed Collagen	11.60	N/A	30.17	N/A

Table 4-3 Endurance limit for each phase at global level

Endurance limit for the d/a master SN curve will depend upon the lower value of endurance limit of three different interfaces at global level among the three phases. Similarly the strength of d/a interface will depend upon the phase failing first under a applied loading for only 1 cycle.

	Stress Controlled		Strain Controlled	
	Graded HL	Uniform HL	Graded HL	Uniform HL
Endurance limit(MPa)	11.60	24.42	30.17	35.96
Strength(MPa)	41.12	53.17	97.72	97.72

Table 4-4 Endurance limit and strength for master SN curve for d-a interface

The following example illustrates how the master SN curve for d-a interface is calculated once the strength and endurance limits have been established:

Step 1: Apply a global stress, say 35MPa, and compute local stresses. For the case in which d-a

interface has graded hybrid layer, the local stresses are as follows.

$$\sigma_l^{Adhesive} = \sigma_g f^{adhesive}, f^{adhesive} = 1.50 ; \sigma_l^{Adhesive} = 52.5$$

$$\sigma_l^{Exposed-Collagen} = \sigma_g f^{Exposed-Collagen}, f^{Exposed-Collagen} = 1.04 ; \sigma_l^{Exposed-Collagen} = 36.4$$

$$\sigma_l^{Dentin} = \sigma_g f^{Dentin}, f^{Dentin} = 1.3 ; \sigma_l^{Dentin} = 45.5$$

Step 2: Obtain the number of cycles to failure at local stress level using S-N curves for particular phase as follows:

$$N_{52.5}^{Adhesive} = 18$$

$$N_{36.4}^{Exposed-Collagen} = 28$$

$$N_{45.5}^{Dentin} = 66951$$

The lowest number of cycle to failure will govern. We can see that *adhesive* will be failing first because it has lower number of cycles as compared to exposed collagen and dentin.

Step 3: Repeat steps 1 and 2 for other stress amplitudes between the strength and the endurance limit. For example, when the global stress is 30 MPa then number of cycles to failure at local stress level for particular phase

$$N_{45}^{Adhesive} = 271$$

$$N_{31.2}^{Exposed-Collagen} = 120$$

$$N_{39}^{Dentin} = 5.61\text{E}+05$$

For this calculation we can see that *exposed collagen* will be failing first because it has lower number of cycles as compared to exposed collagen and dentin.

Steps 1 through 3 were applied for both strain and stress loading conditions on d-a interface and the master S-N curves were obtained as shown in Figures 4-5 and tabulated in table 4-5 through 4-8.

Global Stress	Local Stresses			Number of Cycles			Minimum Cycles	Failing phase
	Adhesive	Collagen	Dentin	Adhesive	collagen	dentin		
9.1	13.65	9.47	11.83	4.31E+11	1.01E+07	7.85E+12	1.01E+07	No Failure
11.6	17.40	12.07	15.09	5.75E+09	1.00E+06	2.75E+11	1.00E+06	Collagen
12	18	12.48	15.6	3.17E+09	7.27E+05	1.73E+11	7.27E+05	Collagen
13	19.5	13.52	16.9	7.64E+08	3.40E+05	5.73E+10	3.40E+05	Collagen
14	21	14.56	18.2	2.05E+08	1.68E+05	2.06E+10	1.68E+05	Collagen
15	22.5	15.6	19.5	6.02E+07	87176	7.97E+09	87176	Collagen
16	24	16.64	20.8	1.91E+07	47202	3.27E+09	47202	Collagen
17	25.5	17.68	22.1	6.51E+06	26527	1.42E+09	26527	Collagen
18	27	18.72	23.4	2.36E+06	15407	6.44E+08	15407	Collagen
19	28.5	19.76	24.7	9.03E+05	9215	3.06E+08	9215	Collagen
20	30	20.8	26	3.63E+05	5659	1.51E+08	5659	Collagen
21	31.5	21.84	27.3	1.53E+05	3559	7.69E+07	3559	Collagen
22	33	22.88	28.6	66836	2287	4.05E+07	2287	Collagen
23	34.5	23.92	29.9	30347	1499	2.19E+07	1499	Collagen
24	36	24.96	31.2	14250	1000	1.22E+07	1000	Collagen
25	37.5	26	32.5	6901	679	6.94E+06	679	Collagen
26	39	27.04	33.8	3438	467	4.04E+06	467	Collagen
27	40.5	28.08	35.1	1759	326	2.40E+06	326	Collagen
28	42	29.12	36.4	922	231	1.45E+06	231	Collagen
29	43.5	30.16	37.7	494	166	8.96E+05	166	Collagen
30	45	31.2	39	271	120	5.61E+05	120	Collagen
31	46.5	32.24	40.3	151	88	3.57E+05	88	Collagen
32	48	33.28	41.6	86	65	2.30E+05	65	Collagen
33	49.5	34.32	42.9	50	48	1.51E+05	48	Collagen
34	51	35.36	44.2	29	36	99862	29	Adhesive
35	52.5	36.4	45.5	18	28	66951	18	Adhesive
36	54	37.44	46.8	11	21	45395	11	Adhesive
37	55.5	38.48	48.1	7	16	31108	7	Adhesive
38	57	39.52	49.4	4	13	21534	4	Adhesive
39	58.5	40.56	50.7	3	10	15050	3	Adhesive
40	60	41.6	52	2	8	10614	2	Adhesive
41.12	61.691	42.772	53.46	1	6	7235	1	Adhesive

Table 4-5 Master SN curve calculation in stress controlled -Graded HL

Global Stress	Local Stresses		Number of cycles		Minimum Cycles	Failing Phase
	Adhesive	Dentin	Adhesive	Dentin		
21.45	24.882	27.885	1.01E+07	5.74E+07	1.01E+07	Adhesive
24.429	28.338	31.758	1.00E+06	9.54E+06	1.00E+06	Adhesive
25	29	32.5	6.63E+05	6.94E+06	6.63E+05	Adhesive
26	30.16	33.8	3.31E+05	4.04E+06	3.31E+05	Adhesive
27	31.32	35.1	1.69E+05	2.40E+06	1.69E+05	Adhesive
28	32.48	36.4	88620	1.45E+06	88620	Adhesive
29	33.64	37.7	47516	8.96E+05	47516	Adhesive
30	34.8	39	26021	5.61E+05	26021	Adhesive
31	35.96	40.3	14534	3.57E+05	14534	Adhesive
32	37.12	41.6	8269	2.30E+05	8269	Adhesive
33	38.28	42.9	4787	1.51E+05	4787	Adhesive
34	39.44	44.2	2817	99862	2817	Adhesive
35	40.6	45.5	1684	66951	1684	Adhesive
36	41.76	46.8	1021	45395	1021	Adhesive
37	42.92	48.1	627	31108	627	Adhesive
38	44.08	49.4	391	21534	391	Adhesive
39	45.24	50.7	246	15050	246	Adhesive
40	46.4	52	157	10614	157	Adhesive
41	47.56	53.3	101	7550	101	Adhesive
42	48.72	54.6	66	5415	66	Adhesive
43	49.88	55.9	43	3914	43	Adhesive
44	51.04	57.2	29	2851	29	Adhesive
45	52.2	58.5	19	2091	19	Adhesive
46	53.36	59.8	13	1544	13	Adhesive
47	54.52	61.1	9	1148	9	Adhesive
48	55.68	62.4	6	858	6	Adhesive
49	56.84	63.7	4	646	4	Adhesive
50	58	65	3	489	3	Adhesive
51	59.16	66.3	2	372	2	Adhesive
53.17	61.677	69.121	1	209	1	Adhesive

Table 4-6 Master SN curve calculation in stress controlled-Uniform HL

Global Stress	Local Stress			Number of Cycles			Minimum Cycles	Failing Phase
	Adhesive	Collagen	Dentin	Adhesive	Collagen	Dentin		
23.68	8.0038	9.48	24.627	5.66E+15	1.00E+07	3.18E+08	1.00E+07	No Failure
30.17	10.197	12.09	31.377	7.66E+13	1.00E+06	1.13E+07	1.00E+06	Collagen
31	10.478	12.4	32.24	4.73E+13	7.73E+05	7.75E+06	7.73E+05	Collagen
32	10.816	12.8	33.28	2.69E+13	5.72E+05	5.00E+06	5.72E+05	Collagen
33	11.154	13.2	34.32	1.56E+13	4.27E+05	3.27E+06	4.27E+05	Collagen
34	11.492	13.6	35.36	9.16E+12	3.21E+05	2.17E+06	3.21E+05	Collagen
35	11.83	14	36.4	5.48E+12	2.44E+05	1.45E+06	2.44E+05	Collagen
36	12.168	14.4	37.44	3.32E+12	1.87E+05	9.86E+05	1.87E+05	Collagen
37	12.506	14.8	38.48	2.04E+12	1.44E+05	6.75E+05	1.44E+05	Collagen
38	12.844	15.2	39.52	1.27E+12	1.12E+05	4.68E+05	1.12E+05	Collagen
39	13.182	15.6	40.56	8.01E+11	87176	3.27E+05	87176	Collagen
40	13.52	16	41.6	5.11E+11	68529	2.30E+05	68529	Collagen
45	15.21	18	46.8	6.31E+10	22368	45395	22368	Collagen
50	16.9	20	52	9.71E+09	8216	10614	8216	Collagen
55	18.59	22	57.2	1.79E+09	3321	2851	2851	Dentin
60	20.28	24	62.4	3.81E+08	1452	858	858	Dentin
65	21.97	26	67.6	9.19E+07	679	285	285	Dentin
70	23.66	28	72.8	2.46E+07	335	102	102	Dentin
75	25.35	30	78	7.23E+06	174	40	40	Dentin
80	27.04	32	83.2	2.30E+06	94	16	16	Dentin
85	28.73	34	88.4	7.83E+05	53	7	7	Dentin
95	32.11	38	98.8	1.09E+05	18	2	2	Dentin
97.72	33.029	39.088	101.63	65788	14	1	1	Dentin

Table 4-7 Master SN curve calculation in strain controlled- Graded HL

Global Stress	Local Stress		Number of Cycles		Minimum Cycles	Failing Phase
	Adhesive	Dentin	Adhesive	Dentin		
30.43	10.164	31.647	8.12E+13	1.00E+07	1.00E+07	No Failure
35.89	11.987	37.326	4.33E+12	1.03E+06	1.03E+06	Dentin
36	12.024	37.44	4.10E+12	9.86E+05	9.86E+05	Dentin
37	12.358	38.48	2.52E+12	6.75E+05	6.75E+05	Dentin
38	12.692	39.52	1.57E+12	4.68E+05	4.68E+05	Dentin
39	13.026	40.56	9.90E+11	3.27E+05	3.27E+05	Dentin
40	13.36	41.6	6.31E+11	2.30E+05	2.30E+05	Dentin
45	15.03	46.8	7.79E+10	45395	45395	Dentin
50	16.7	52	1.20E+10	10614	10614	Dentin
55	18.37	57.2	2.21E+09	2851	2851	Dentin
60	20.04	62.4	4.70E+08	858	858	Dentin
65	21.71	67.6	1.14E+08	285	285	Dentin
70	23.38	72.8	3.04E+07	102	102	Dentin
75	25.05	78	8.94E+06	40	40	Dentin
80	26.72	83.2	2.84E+06	16	16	Dentin
85	28.39	88.4	9.68E+05	7	7	Dentin
95	31.73	98.8	1.34E+05	2	2	Dentin
97.72	32.638	101.63	81280	1	1	Dentin

Table 4-8 Master SN curve calculation in strain controlled- Uniform HL layer properties

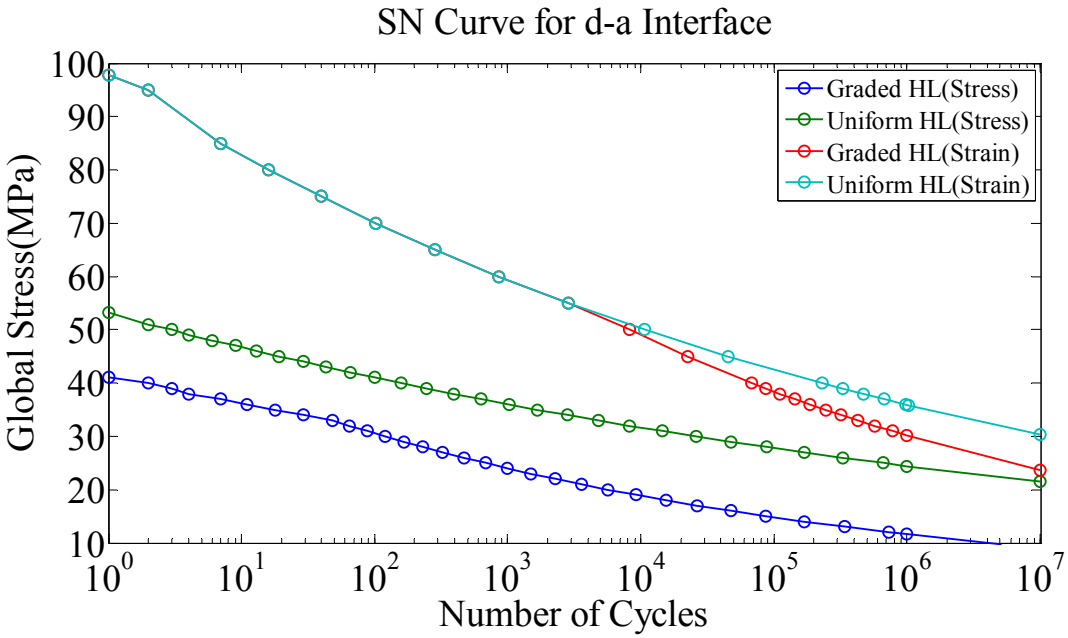

Figure 4:5 Master SN curves for d-a interface in different conditions

5.0 DISCUSSION

5.1 MECHANICAL TESTING AND VISCOELASTIC MODELING

In the current study we have performed creep, stress-strain and fatigue experiments on dentin adhesives in both dry and wet conditions. Stress-strain tests were performed at three different loading rates, 10N/min, 0.1N/min and 0.0075N/min. Dentin adhesives have different elastic moduli at different loading rates, e.g. 2.42GPa at 0.0075N/min, 3.06GPa at 0.1N/min and 3.53GPa at 10N/min under dry conditions as shown in Table 2-2. For the wet condition elastic moduli for three loading rates were 1.04GPa at 0.0075N/min, 1.46GP at 0.1N/min and 1.62 at 10N/min shown in Table 2-3. Further if we compare dentin adhesive in wet and dry conditions, the material is very weak (both in elastic modulus and flexural strength) in the wet condition based on the stress-strain data (Figure 2:9 and 2:10). At loading rate of 0.1N/min and under wet conditions, the dentin adhesives have an elastic modulus of approximately 1.46GPa, but the same material at similar loading rate under dry conditions has an elastic modulus approx 3.06GPa. There is nearly 50% reduction in the elastic modulus under wet conditions. The flexural strength also decreases from ~160 MPa in dry case to ~60MPa in wet case for 10N/min loading rate. Creep tests were performed because dentin adhesives are polymeric materials which are viscoelastic in nature. Creep tests were performed in both dry and wet conditions at 4 different stress levels. Creep behavior for both wet and dry testing was nearly linear for the lower three stress values. The creep behavior at stress levels of 80MPa in dry adhesive (Figure 2:5) and 30.5MPa in wet

adhesive (Figure 2:6) was nonlinear with respect to stress applied. Figures 2:5 and 2:6 show that both wet and dry samples have very large strains 7-7.5% which corresponds to plastic deformation in the samples (based upon stress-strain curves). For these large stress levels the samples did not recover to its original state; the samples exhibited features associated with large residual strain (samples permanently bended) once the applied stress was removed.

The viscoelastic model used in this study is linear, hence for the calculation of the viscoelastic model parameters only linear creep data is used (lower three stress level in both wet and dry conditions). In the viscoelastic model because of the complex nature of the dentin adhesive we chose 5 different retardation times in 0.1, 100, 1000, 10000 and 100000 seconds. Creep data were fitted using nonlinear least square method to calculate the creep constants. While performing least-square fitting, care is taken so that all creep constants are non-negative. Non-negative coefficients [22-23] lead to decrease of strain with time even when constant stress is maintained. There are many methods to avoid non-negative coefficients while fitting creep data like interactive adjustment of relaxation or retardation times [24], recursive algorithm [25] or power law presmoothing[26].

Fatigue tests were performed at the frequency of 5 Hz and at the stress ratio of R=0.1 while the temperature was maintained at 37^{o} C. Strain in the fatigue testing is composed of two parts, (1) strain due the creeping of sample under the mean stress and (2) strain due to damage accumulation because of cyclic loading. At stress amplitude of 30MPa in dry conditions (Figure 2:11) and 10MPa in wet condition (Figure 2:15) there is not much contribution of strain from damage accumulation. Rather most of the strain is due to creeping of sample under mean stress of 36.6MPa and 12.22MPa for dry and wet testing, respectively. Moreover our model is linear viscoelastic which does not take into account the damage accumulation hence strain versus time predicted curves and actual curves are very close for the lower stress amplitude testing in dry and wet conditions. For a stress amplitude of

45MPa in dry testing (Figure 2:14) and 25MPa in wet conditions (Figure 2:18), the predicted curves are close to the experimental curves in the beginning, but as the time proceeds both the curves deviate from the experimental curves. This deviation can be explained by damage accumulation that occurs with time due to cycling at higher stress levels. The predicted curves do not account for this damage accumulation rather they show the behavior of the adhesive specimens under mean stress of 55MPa and 30.5MPa for dry and wet testing respectively.

For the calculation of fatigue life at particular stress amplitude, we chose two different criteria for failure in fatigue as described in the section 2.6.4. From the Table 2.4 we can see that, when the failure strain is 2.1%, adhesive sample at stress amplitude of 45MPa will only last for average 1679 cycles with standard deviation of 402. But, at 30MPa, adhesive specimen will last for average 67043 cycles with very high standard deviation of 54877. For all strain criteria the standard deviation becomes larger with a decrease in stress amplitude, i.e., there is a large variation in the fatigue life of adhesive specimens at smaller stress amplitudes. Secondly the sample has a longer fatigue life with higher failure strain. If we compare the data in Table 2-4 and 2-5 for 2.3% strain criteria, 30MPa dry specimens has very long fatigue life, about 147861 cycles. But wet adhesive samples at 25 MP stress amplitude have average life of about 163 cycles.

5.2 FINITE ELEMENT ANALYSIS

3d finite element model of computational unit cell of d-a interface is developed because it gives more realistic and reliable results then 2d finite element model. In the present study we have used linear elastic properties for different material components in the d-a interface, but in actuality the materials could be nonlinear and viscoelastic. The model was

subjected to two types of boundary conditions (1) stress controlled (2) strain controlled because in real conditions loading is in between stress and stain. Hence it was important to study the behavior of unit cell under two types of boundary conditions.

If we compare the four different models in Figure 3:9, the unit cell with uniform hybrid layer has less stress concentration in the adhesive tags as compared to the unit cell with a graded hybrid layer, because uniform hybrid layer has homogeneous elastic properties along its depth. Secondly when the hybrid layer is short (Figure 3:9(3)), there are reduction in stress values as compared with a graded hybrid layer. The stress distributions in the unit cell that does not contain a zone of partially demineralized dentin (Figure 3:9(4)) and the unit cell with a graded hybrid layer are almost same. Further, stress distribution in exposed collagen of graded hybrid layer (Figure 3:10(1)) and short hybrid layer (Figure 3:10(3)) is similar. But, exposed collagen in unit cell with no partially demineralized dentin (Figure 3:10(4)) has slightly lower stresses as compared to unit cell with graded hybrid layer. Lastly stress distribution in the intertubular dentin and peritubular dentin (Figure 3:11) is almost same in all the four different models.

Stress controlled loading (Figure 3:9) showed higher stress concentration in adhesive tags as compared to dentin and other phases, hence in this case adhesive tags are more prone to failure due to relatively higher stress. In comparison, under strain controlled (Figure 3:16) loading, the adhesive tag had relatively lower stresses as compared to dentin and other phases. Hence the adhesive tag is experiencing stress shielding. Stress concentration in the graded hybrid layer under stress and strain loading were approximately 1.5 and 0.35 respectively. These results suggest that the mean stress experienced by the adhesive tag under masticatory function could vary from 1.5 to 0.35 times the applied load.

From the results of the stress controlled case we can conclude that the adhesive tag is more prone to failure because it experiences the larger stresses due to complex geometry and

relative softer properties compared to other phases in the unit cell. The condition become worse when there is a defect present in the form of a cavity (spherical cavity in our case). Moreover a dentin-adhesive interface that possesses a thin hybrid layer with uniform material properties experiences smaller and more uniform stresses as compared to a thick hybrid layer with graded properties.

5.3 FATIGUE LIFE PREDICTION OF D-A INTERFACE

For the fatigue life prediction of d-a interface it is very important to have accurate S-N curves for the different material components. Due to the lack of data only three phases, exposed-collagen, dentin and adhesive were used in this study to demonstrate the methodology. Stress concentration for the three different phases were calculated based upon the finite element analysis. Moreover, the methodology for fatigue life prediction in this study is based upon isolated computational unit cell having periodic boundary conditions. But, under actual clinical function, the unit cell for the d-a interface will have both strain and stress boundary conditions. Hence it is important to consider two extreme case of loading which can give upper and lower bounds in terms of fatigue life for the d-a interface

We have shown the methodology for the two extreme cases of geometries (1) when the hybrid layer has uniform material properties (2) and when hybrid layer has graded material properties along its depth. Tables 4-5 to 4-8 shows the calculated S-N data for d-a master curve in graded and uniform hybrid layer under stress and strain loadings. Under the stress controlled loading, adhesive has shortest fatigue life at higher stress amplitudes, whereas, at lower stress amplitudes, either exposed-collagen or adhesive could fail depending upon microstructure of hybrid layer. On the other hand, under strain controlled loading

dentin has shortest fatigue at higher stress amplitudes. Under strain loading the adhesive does not fail because of stress shielding.

All the S-N data for stress and strain loading is shown in Figure 4:5. If we compare the four S-N curves, the d-a interface with graded hybrid layer under stress controlled loading has the lowest fatigue life which gives lower limit for the fatigue behavior of d-a interface. On the other hand, the d-a interface with uniform hybrid layer under strain controlled loading has longest fatigue life which gives the upper bound for the fatigue behavior of d-a interface. Figure 4:6 shows predicted curve along with measured curve [5] for the dentin-composite interface. The measured curve falls in the stress controlled region because the authors have performed the experiment on small rectangular beam samples which have smaller number of unit cells as compared to the actual d-a interface. Fewer unit cells mean less constraint in the lateral direction. Hence d-a unit cell in their study could be experiencing stress boundary conditions without constraint in the lateral direction, therefore the measured S-N curve falls in the region of stress controlled loading.

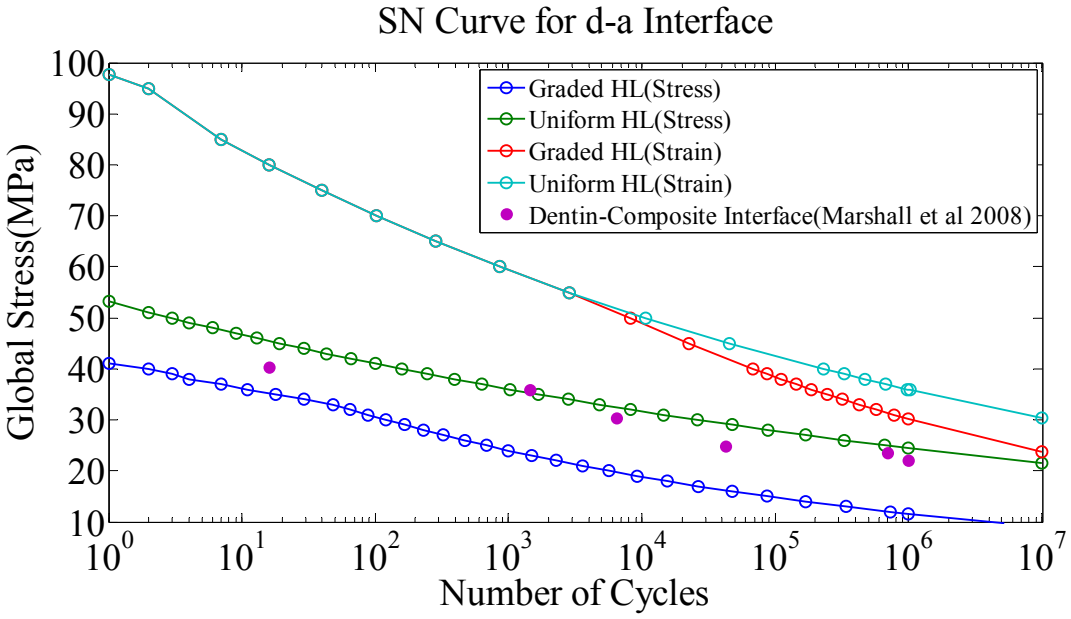

Figure 5:1 Master SN curves for d-a interface along with measured data [5]

6.0 CONCLUSION & FUTURE WORK

6.1 CONCLUSIONS

Creep, static and fatigue tests were performed for a model dentin adhesive. Adhesive elastic modulus depends upon the rate of loading in addition to the temperature. Secondly, strength and elastic modulus of model dentin adhesives are reduced by nearly one-half when tested under wet conditions. This difference is likely due to the plasticizing effect of water. The viscoelastic model was able to predict the elastic modulus which was very close to measured elastic modulus. Creep tests and viscoelastic model showed that the model dentin adhesive is a complex viscoelastic material. Hence at least creep tests must be performed to characterize the viscoelastic properties of dentin adhesives. Fatigue tests showed that dentin adhesive in dry conditions have considerably longer durability than adhesives in wet conditions under constant stress cyclic loading.

3d finite element model of the d-a interface showed that under stress controlled loading, adhesive tags are more prone to failure, because of higher and non-uniform stresses as compared to other phases. Because of higher stresses, failure could initiate through the adhesive tag. Stress distribution is largely effected by the hybrid layer properties, when a uniform hybrid layer is formed, the adhesive tags experience smaller stresses as compared to the graded hybrid layer. Thin hybrid layers experience less stress than thick hybrid layers. Hence unit cells with thinner, uniform hybrid layer will experience smaller stress concentration. Stress distributions in exposed collagen, peritubular dentin and intertubular

were not effected by hybrid layer properties. Finite element calculations under the strain controlled case showed smaller stresses in adhesive tags and larger stresses in dentin. Hence in this case the adhesive experiences stress shielding and there is less chance that the failure will initiate in the adhesive or adhesive tag.

Master S-N curve for d-a interface showed a strong dependence upon type of loading and hybrid layer properties. Dentin-adhesive interface with graded hybrid layer under stress controlled loading had shortest fatigue life whereas the d-a interface with uniform hybrid layer under strain controlled loading had longest fatigue life. In both the stress and strain controlled cases the d-a interface with uniform hybrid layer showed longer fatigue life as compared to d-a interface with graded hybrid layer.

6.2 FUTURE WORK

In the present study we have performed mechanical testing on one type of dentin adhesive only. To better understand behavior of dentin adhesives we need to perform similar types of studies on other types of dentin adhesives. Moreover, in the future we need to study stress-strain behavior at other loading rates. The creep tests were performed for just 120 minutes, but to better fit the viscoelastic model we need to perform the creep tests for longer times. Secondly in the present study we used the linear viscoelastic model to predict the mechanical behavior of the dentin adhesive. But, we have seen in the study that the adhesive is not a linear viscoelastic material, hence we need a nonlinear viscoelastic model. In the current study fatigue tests were performed at frequency of 5Hz, because these materials have frequency dependence behavior, in the future we need to perform fatigue tests at different frequencies.

The current 3d finite element model has linear-elastic properties, but the dentin adhesive is not linear elastic, hence in the future we need to model d-a interface using nonlinear and viscoelastic elements. Moreover in the current study, the computational model of d-a interface is subjected to uni-axial tensile loading, but under real-world conditions the loading is rather multi-axial. So in the future to fully understand the overall behavior of the d-a interface we need to investigate the behavior of the computational unit cell under shear loading as well as uniaxial tensile. For the fatigue life prediction we have used only three phases, dentin, collagen and adhesive. But, for accurate calculation of S-N curve of d-a interface we need S-N curve of, partially demineralized dentin, and hybrid layers. S-N curve for, partially demineralized dentin and hybrid layers are not available in the current literature. To find the S-N curves mechanical testing (static, creep and fatigue) should be performed on hybrid layers; these hybrid layers would be represented by composites of adhesive and collagen in different ratios. Secondly the overall fatigue behavior of the d-a interface cannot be governed by the fatigue behavior of d-a interface in uniaxial tensile loading alone. So fatigue behavior of d-a interface under shear loading should be studied and combined with tensile fatigue behavior to give overall fatigue life of d-a interface.

REFRENCES

1. Beazoglou T, Eklund S, Heffley D, Meiers J, Brown LJ, Bailit H. Economic impact of regulating the use of amalgam restorations. Public Health Rep 2007;122(5):657-63.
2. Murray PE, Windsor LJ, Smyth TW, Hafez AA, Cox CF. Analysis of pulpal reactions to restorative procedures, materials, pulp capping, and future therapies. Crit Rev Oral Biol Med 2002;13(6):509-20.
3. Lohbauer U, Frankenberger R, Kramer N, Petschelt A. Strength and fatigue performance versus filler fraction of different types of direct dental restoratives. J Biomed Mater Res B Appl Biomater 2006;76(1):114-20.
4. Drummond JL. Degradation, fatigue, and failure of resin dental composite materials. J Dent Res 2008;87(8):710-9.
5. Staninec M, Kim P, Marshall GW, Ritchie RO, Marshall SJ. Fatigue of Dentin-Composite Interface with Four-Point Bend. Dental Materials 2008 24 799-803
6. Shah MB, Ferracane JL, Kruzic JJ. Mechanistic aspects of fatigue crack growth behavior in resin based dental restorative composites. Dental Materials 2009;25:909-16.
7. Wang XT, Ker RF, Alexander RM. Fatigue Rupture of Wallaby Tail Tendons The Journal of Experimental Biology 1995;198:847-52.
8. Nalla RK, Imbeni V, Kinney JH, Staninec M, Marshall SJ, Ritchie RO. In Vitro Fatigue Behavior of Human Dentin with Implications for Life Prediction. Journal of Biomedical Material Research 2003;66A:10-20.

9. Nalla RK, Kinney JH, Marshall SJ, Ritchie RO. On the in vitro Fatigue Behavior of Human Dentin: Effect of Mean Stress. Journal of Dental Research 2004;83(3).

10. Rodrigues FP, Li J, Sliikas N, Ballester RY, Watts DC. Sequential Software Processing of micro-XCT Dental Images for 3D-FE Analysis Dental Materials 2009.

11. Wakabayashi N, Ona M, Suzuki T, Igarashi Y. Nonlinear finite element analyses: advances and challenges in dental applications. J Dent 2008;36(7):463-71.

12. Yettram AL, Wright KWJ, Pickard HM. Finite Element Stress Analysis of the Crowns of Normal and Restored Teeth. J Dent Res 1976:104-1011.

13. Ausiello P, Apicella A, Davidson CL. Effect of Adhesive Layer Properties on Stress Distribution in Composite Restoration- a 3D Finite element Analysis Dental Materials 2002;18:295-303.

14. Frankenberger R, Strobel WO, Kramer N, Lohbauer U, Winterscheidt J, Winterscheidt B, et al. Evaluation of the Fatigue Behavior of the Resin-Dentin Bond with the Use of Different Methods. Journal of Biomedical Material Research Part B 2003;67B:712-21.

15. Frankenberger R, Kramer N, Petschelt A. Fatigue Behavior of Different Dentin Adhesives Clincal Oral Investigations 1999;3:11-17.

16. Draughn RA. Compressive Fagtiue Limits of Composite Restorative Materials Journal of Dental Research 1979;58(3):1093-96.

17. Park JG, Ye Q, Topp EM, Lee CH, Kostoryz EL, Misra A, et al. Dynamic mechanical analysis and esterase degradation of dentin adhesives containing a branched methacrylate. J Biomed Mater Res B Appl Biomater 2009;91(1):61-70.

18. Santis AD, Baldi M. Photo-Polymerization of Composite Resins Measured by Micro-Raman Spectroscopy. Polymer 2004;45:3797-804.

19. Dowling NE. Mechanical Behavior of Materials Prentice Hall; 1993.

20. Wineman AS, Rajagopal KR. Mechanical Response of Polymers: Cambridge University Press; 2000.

21. Haddad YM. Viscoelasticity of Engineering Materials Chapman & Hall; 1995.

22. Chen T. Determining a Prony Series for a Viscoelastic Material from Time Varying Strain Data. U.S Army Research Laboratory 2000.

23. Dooling PJ, Buckley CP, Hinduja S. An Intermediate Model Method for Obtaining a Discrete Relaxation Spectrum from Creep Data. Rheological Acta 1997;36:472-82.

24. Baumgaertel M, Winter HH. Determination of Discrete Relaxation and Retardation Time Spectra from Dynamic Mechanical Data. Rheological Acta 1989;28:511-19.

25. Tschoegl NW, Emri I. Generating Line Spectra from Experimental Response Part III: Interconversion Between Relaxation and Retardation Behavior. . Int J Polymerica Mat 1992;18:117-27.

26. Park SW, Kim YR. Fitting Prony-Series Viscoelastic Models with Power-Law Presmoothing. . Journal of Materials in Civil Engineering 2001;13(1).

27. Butler WT. Dentin extracellular matrix and dentinogenesis. Oper Dent 1992;Suppl 5:18-23.

28. Wang R, Weiner S. Human root dentin: structural anisotropy and Vickers microhardness isotropy. Connect Tissue Res 1998;39(4):269-79.

29. Marangos O, Misra A, Spencer P, Bohaty B, Katz JL. Physico- mechanical properties determination using microscale homotopic measurment: Application to sound and caris-affected tooth dentin Acta Biomater 2008.

30. Koutsi V, Noonan RG, Horner JA, Simpson MD, Matthews WG, Pashley DH. The effect of dentin depth on the permeability and ultrastructure of primary molars. Pediatr Dent 1994;16(1):29-35.

31. Wang Y, Spencer P. Overestimating hybrid layer quality in polished adhesive/dentin interfaces. J Biomed Mater Res A 2004;68(4):735-46.

32. Wang Y, Spencer P. Quantifying adhesive penetration in adhesive/dentin interface using confocal Raman microspectroscopy. J Biomed Mater Res 2002;59(1):46-55.

33. Misra A, Spencer P, Marangos O, Wang Y, Katz JL. Parametric Study of the Effect of Phase Anisotropy on the Micromechanical Behavior of dentin-adhesive Interface. Journal of Royal Society Interface 2005;2.

34. Katz JL, Bumrerraj S, Dreyfuss J, Wang Y, Spencer P. Micromechanics of the dentin/adhesive interface. J Biomed Mater Res 2001;58(4):366-71.

35. Wieliczka DM, Kruger MB, Spencer P. Raman imaging of dental adhesive diffusion. Appl. Spectrosc 1997;51:1593–96.

36. Wieliczka DM, Spencer P, Kruger MB. Raman mapping of the dentin/adhesive interface. Appl. Spectrosc 1996;50:1500–04.

37. Misra A, Spencer P, Marangos O, Wang Y, Katz JL. Micromechanical Analysis of Dentin/Adhesive Interface by the Finite Element Method. J Biomed Mater Res Part B: Appl Biomater 2004;70B:56-65.

38. Katz JL, Spencer P, Nomura T, Wagh A, Wang Y. Micromechanical properties of demineralized dentin collagen with and without adhesive infiltration. J Biomed Mater Res A 2003;66(1):120-8.

39. Kinney JH, Balooch M, Marshall GW, Marshall SJ. A micromechanics model of the elastic properties of human dentine. Arch Oral Biol 1999;44(10):813-22.

40. Nasser SN, Hori M. Micromechanics: Overall Properties of Heterogeneous Materials Elsevier; 1999.